

**DEVELOPMENT OF BATTERY CHARGING
STATION FOR AUTOMATED GUIDED VEHICLE**

TAN TAR WEI

UNIVERSITI TUNKU ABDUL RAHMAN

**DEVELOPMENT OF BATTERY CHARGING STATION FOR
AUTOMATED GUIDED VEHICLE**

TAN TAR WEI

**A project report submitted in partial fulfilment of the
requirements for the award of Bachelor of Engineering
Mechatronics Engineering with Honours**

**Lee Kong Chian Faculty of Engineering and Science
Universiti Tunku Abdul Rahman**

May 2023

DECLARATION

I hereby declare that this project report is based on my original work except for citations and quotations which have been duly acknowledged. I also declare that it has not been previously and concurrently submitted for any other degree or award at UTAR or other institutions.

Signature : *TanWei*

Name : Tan Tar Wei

ID No. : 1801086

Date : 2.5.2023

APPROVAL FOR SUBMISSION

I certify that this project report entitled “**DEVELOPMENT OF BATTERY CHARGING STATION FOR AUTOMATED GUIDED VEHICLE**” was prepared by **TAN TAR WEI** has met the required standard for submission in partial fulfilment of the requirements for the award of Bachelor of Mechatronics Engineering with Honours at Universiti Tunku Abdul Rahman.

Approved by,

Signature : 

Supervisor : Dr. Hau Lee Cheun

Date : 2.5.2023

Signature : 

Co-Supervisor : Dr. Danny Ng Wee Kiat

Date : 2.5.2023

The copyright of this report belongs to the author under the terms of the copyright Act 1987 as qualified by Intellectual Property Policy of Universiti Tunku Abdul Rahman. Due acknowledgement shall always be made of the use of any material contained in, or derived from, this report.

© 2023, Tan Tar Wei. All right reserved.

ACKNOWLEDGEMENTS

I would like to thank everyone who had contributed to the successful completion of this project. I would like to express my gratitude to my research supervisor, Dr. Hau Lee Cheun and Dr. Danny Ng Wee Kiat for their invaluable advice, guidance and their enormous patience throughout the development of the research.

In addition, I would also like to express my gratitude to my loving parents and friends who had helped and given me encouragement to continue this journey.

ABSTRACT

The use of Automated Guided Vehicles (AGVs) has been instrumental in transitioning industries from traditional labor-based to automation. Lithium-ion batteries are the primary energy storage devices used in AGVs, owing to their higher energy density and longer cycle life compared to other types of cells (Fuqiang *et al.*, 2019). However, the charging and discharging of these batteries require proper precautions to avoid affecting their performance and lifespan. This project aimed to develop a battery charging station for AGVs that are able to charge lithium-ion batteries optimally. Firstly, the main charger (DPS5015) was modified to enable autonomous control via an Arduino microcontroller. Next, the charging station incorporated the concept of the Internet of Things (IoT) by visualizing and storing the charging data on a web server named Cayenne. Additionally, the charger was equipped with a state-of-charge (SoC) estimator that utilized coulomb counting to estimate the battery's SoC. Upon completion, the battery charging station's prototype proves its flexibility by performing constant current - constant voltage (CC-CV) charging at 0.2C (0.6A) termination criteria and multistage constant current (MSCC) charging profile at 5.4A - 4.1A - 2.8A - 1.6A - 0.6A. Moreover, the IoT data management function by Cayenne stored thousands of charging data with no issues. On the other hand, the SoC estimator had an error of 7.16% when tested under the external discharging circuit. The accuracy of the SoC estimator was acceptable as most industrial SoC estimators were only able to indicate the SoC at 20% or 25% intervals. Finally, a comparison was made between CC-CV and MSCC charging profiles using hardware experimentation data obtained during the charging process, showing that both profiles have similar charging times, but MSCC charging is better for the battery's health.

TABLE OF CONTENTS

DECLARATION		i
APPROVAL FOR SUBMISSION		ii
ACKNOWLEDGEMENTS		iv
ABSTRACT		v
TABLE OF CONTENTS		vi
LIST OF TABLES		ix
LIST OF FIGURES		x
LIST OF SYMBOLS / ABBREVIATIONS		xiv
LIST OF APPENDICES		xv
CHAPTER		
1	INTRODUCTION	1
1.1	General Introduction	1
1.2	Importance of the Study	1
1.3	Problem Statement	2
1.4	Aim and Objectives	2
1.5	Scope and Limitation of the Study	2
1.6	Contribution of the Study	3
1.7	Outline of the Report	3
2	LITERATURE REVIEW	5
2.1	Introduction	5
2.2	Mechanical Design	5
2.2.1	Contact and Contactless charging methods	5
2.2.2	Comparison between contact and contactless charging	6
2.3	Electrical Design	7
2.3.1	Battery Charger	7
2.3.2	AC/DC converter	8

2.3.3	Examples of AC/DC switching mode power supply	9
2.3.4	DC/DC Converter	13
2.3.5	Example of DC/DC design	14
2.4	Charging profile	17
2.4.1	Constant voltage(CV) charging	18
2.4.2	Constant current - Constant voltage (CC-CV) charging	18
2.4.3	Multiple Stage Constant Current (MSCC) charging	20
2.4.4	Comparison between CC-CV and MSCC	21
2.5	Summary	22
3	METHODOLOGY AND WORK PLAN	23
3.1	Introduction	23
3.2	Prototype design	23
3.2.1	Prototype's components	24
3.2.2	Building prototype	25
3.2.3	BMS	25
3.2.4	Voltage sensor & Current sensor	27
3.2.5	Modify DPS5015	28
3.2.6	SoC estimation	30
3.2.7	UART communication between Arduino and ESP32	31
3.2.8	Communicating with Cayenne	32
3.3	Flowchart for charger operation	32
3.4	Using charger to perform CC-CV and MSCC charging	35
3.5	Testing the charger	35
3.6	Gantt Chart	35
3.7	Summary	37
4	RESULTS AND DISCUSSION	38
4.1	Introduction	38
4.2	Part 1 Result: Prototype	38
4.2.1	Battery charging station hardware	38

4.2.2	IoT data management	40
4.2.3	Autonomous charging parameter adjustment	40
4.2.4	SoC estimator	41
4.3	Part 1 Discussion	43
4.3.1	Battery charging station's prototype	43
4.3.2	Autonomous charging parameter adjustment	45
4.3.3	SoC estimation	45
4.4	Part 2 Result: CC-CV and MSCC charging profil	47
4.5	Part 2 Discussion	54
4.5.1	CC-CV charging	54
4.5.2	MSCC charging	54
4.5.3	Comparison between CC-CV and MSCC charging	55
4.6	Summary	56
5	CONCLUSIONS AND RECOMMENDATIONS	57
5.1	Conclusions	57
5.2	Recommendations for future work	58
	REFERENCES	59
	APPENDICES	63

LIST OF TABLES

Table 4.1:	SoC for charging and discharging process	43
Table 4.2:	CC-CV charging result	50
Table 4.3:	MSCC charging result	53
Table 4.4:	MSCC charging interval	54

LIST OF FIGURES

Figure 2.1:	Contact charging (Super User, n.d.)	5
Figure 2.2:	Contactless charging (Super User, n.d.)	6
Figure 2.3:	Contact charging alignment(Super User, n.d.)	7
Figure 2.4:	Contactless charging alignment(Super User, n.d.)	7
Figure 2.5:	Basic battery charger block diagram	8
Figure 2.6:	Block diagram of switching mode power supply	9
Figure 2.7:	DER 453 schematic diagram (Powerint, 2016)	9
Figure 2.8:	DER 453 Zoom in Input region	10
Figure 2.9:	DER 453 Zoom in Output region	10
Figure 2.10:	DER 453 Zoom in Feedback loop	11
Figure 2.11:	DER 915 schematic diagram (Powerint, 2021)	11
Figure 2.12:	DER 915 Zoom in Input region	12
Figure 2.13:	DER 915 Zoom in Output region	12
Figure 2.14:	DER 915 Zoom in Feedback loop	13
Figure 2.15:	DC/DC converter, Dual feedback loop	14
Figure 2.16:	Chen and Rincon-Mora, Dual feedback loop design (Chen and Rincon-Mora, 2006)	15
Figure 2.17:	Chen and Rincon-Mora, Design application (Chen and Rincon-Mora, 2006)	15
Figure 2.18:	AP4305 schematic (DigiKey, 2022)	16
Figure 2.19:	MP26085 block diagram (DigiKey, 2022)	17
Figure 2.20:	MP26085 design application (DigiKey, 2022)	17
Figure 2.21:	CV, Graph of SOC, Current and Voltage against time (Jha et al., 2022)	18

Figure 2.22:	CC-CV charging profile (Shen, Tu Vo, and Kapoor, 2012)	19
Figure 2.23:	CC-CV, Graph of SOC, Current and Voltage against Time (Jha et al., 2022)	19
Figure 2.24:	MSCC charging profile (Jha et al., 2022)	20
Figure 2.25:	MSCC, Graph of SOC, Current and Voltage against Time(Jha et al., 2022)	21
Figure 3.1:	Complete system prototype	23
Figure 3.2:	3 - cell BMS	26
Figure 3.3:	LiPo battery BMS port voltage	26
Figure 3.4:	XH 2.54 4P male connector	27
Figure 3.5:	XH 2.54 4P female connector	27
Figure 3.6:	Functions corresponding to the 8-pin wire connectors	29
Figure 3.7:	DPS5015 control panel	29
Figure 3.8:	Block diagram for Arduino to DPS5015's connection	30
Figure 3.9:	SoC estimation	31
Figure 3.10:	Cayenne dashboard	32
Figure 3.11:	Coding to establish connection with Cayenne	32
Figure 3.12:	Charging operation	34
Figure 3.13:	Gantt Chart for FYP 1	36
Figure 3.14:	Gantt Chart for FYP 2	36
Figure 4.1:	Charging station prototype	38
Figure 4.2:	Charging station prototype zoom view	39
Figure 4.3:	Charging station prototype zoom view	39
Figure 4.4:	Cayenne's data storage	40
Figure 4.5:	Cayenne data visualization	40

Figure 4.6:	Wire extension from the control panel to Arduino	41
Figure 4.7:	Discharging circuit	42
Figure 4.8:	SoC curve for charging and discharging	42
Figure 4.9:	Voltage (V) and Current (A) vs Time (min) curve for Charging and Discharging process	43
Figure 4.10:	Differences between the current before and after BMS	44
Figure 4.11:	CC-CV CHARGE 1: SOC (%) vs Time (min)	47
Figure 4.12:	CC-CV CHARGE 1: Voltage (v) and Current (A) vs Time (min)	48
Figure 4.13:	CC-CV CHARGE 2: SOC (%) vs Time (min)	48
Figure 4.14:	CC-CV CHARGE 2: Voltage (v) and Current (A) vs Time (min)	49
Figure 4.15:	CC-CV CHARGE 3: SOC (%) vs Time (min)	49
Figure 4.16:	CC-CV CHARGE 3: Voltage (v) and Current (A) vs Time (min)	50
Figure 4.17:	MSCC CHARGE 1: SOC (%) vs Time (min)	51
Figure 4.18:	MSCC CHARGE 1: Voltage (v) and Current (A) vs Time (min)	51
Figure 4.19:	MSCC CHARGE 2: SOC (%) vs Time (min)	52
Figure 4.20:	MSCC CHARGE 2: Voltage (v) and Current (A) vs Time (min)	52
Figure 4.21:	MSCC CHARGE 3: SOC (%) vs Time (min)	53

Figure 4.22: MSCC CHARGE 3: Voltage (v) and Current (A) vs Time
(min)

LIST OF SYMBOLS / ABBREVIATIONS

SoC	State of Charge, %
SoH	State of Health, %
DoD	Depth of Discharge
CC-CV	Constant current – constant voltage charging profile
MSCC	Multiple stage constant current charging profile
CV	Constant voltage charging
CC	Constant current charging
AGV	Automated guided vehicle
IoT	Internet of Things
RX	Receiver
TX	Transmitter
UART	Universal Asynchronous Receiver Transmitter
OCP	Optimum Charging Pattern
LiPo	Lithium Polymer battery

LIST OF APPENDICES

Appendix A: Code and sample excel file from Cayenne	63
---	----

CHAPTER 1

INTRODUCTION

1.1 General Introduction

With the rise of Industry 4.0, many industries are transitioning from traditional labor-based operations to automation, and Automated Guided Vehicles (AGVs) have become a key component in this shift. AGVs are computer-operated load carriers that can move around a facility's floor without requiring an onboard operator or driver. They are widely used in factories to transport raw materials, support production lines, and sort parcels. While some AGVs can recharge themselves automatically, others require human assistance for battery swapping or charging.

A battery charging station is where an AGV charges itself. Designing a battery charging station involves considerations of both mechanical design, the process of connecting the charging station's electrode to the battery, and electrical design, such as power control.

Lithium-ion batteries are one of the main energy storage devices, it has been widely used in electric vehicle (EV), AGVs, medical devices, and more due to their advantages compared with other cells, such as higher energy density and longer cycle life (Fuqiang *et al.*, 2019). Proper precautions must be considered when charging and discharging these batteries as they can affect their performance and lifespan. In this project, a battery charging station was designed to charge LiPo batteries, the charging station was equipped with advanced features such as automated charging current adjustment, State of Charge (SoC) estimation, and the ability to perform both CC-CV and MSCC charging profiles. Additionally, the charging station incorporates the Internet of Things (IoT) concept for efficient data management.

1.2 Importance of the Study

This project develops a highly flexible battery charging station that allows users to charge their batteries with adjustable parameters for faster charging, as well as the option to customize the charging profiles for different battery types. The charging station also includes SoC estimation, which is crucial for evaluating

battery health and benchmarking charger performance. Moreover, by having the SoC data, it provides the user with opportunities to explore different charging profiles for the battery. Additionally, the charging station incorporates IoT for data management, collecting and storing vast amounts of valuable data during the charging and discharging process such as charging and discharging voltage and current, as well as the SoC. These data are collected and stored in real time and can be used for data analysis or preventive maintenance. Overall, this charging station offers increased flexibility and efficiency for battery charging.

1.3 Problem Statement

The current battery charging station for AGV in UTAR has several limitations that need to be addressed. Firstly, the charging station requires manual operation before charging, the user is required to disconnect the charger from AGV and bring it to the charger for charging. Moreover, the charging station also requires manual configuration as users have to adjust the charging parameter manually before every charging and press the start button on the charger to initiate the charging process. These manual processes are not practical for applications with a large number of AGVs. Secondly, there is no SoC estimation to indicate the battery capacity percentage. Additionally, the current charger uses a fixed CC-CV charging profile that cannot be changed, limiting its flexibility. Furthermore, the charger can only charge one battery pack at a time, while the reference AGVs used in the project require two battery packs.

1.4 Aim and Objectives

The aim of this project is to build a battery charging station for AGV and find the best charging profile for the battery.

The objectives are to design and build the charging station with specific features such as autonomous charging parameter adjustment, SoC estimation function, and IoT data management, and to evaluate the charging performance of CC-CV and MSCC charging profiles using the developed charging station.

1.5 Scope and Limitation of the Study

The scope of this study consisted of the entire hardware and software design of the battery charging station which is equipped with IoT data management,

autonomous charging parameter adjustment, and SoC estimation function. Furthermore, the characteristics and performance of two charging profiles: CC-CV and MSCC were studied to find the better charging profile for LiPo batteries.

The limitation of the study was that there was no standard SoC estimator to compare the results for the SoC estimation of the designed charger with. Moreover, there was insufficient equipment to analyze the state-of-health (SoH) of the battery, thus the evaluation of the SoH could not be done.

1.6 Contribution of the Study

This project presents a complete battery charging station for AGVs that offers multiple useful functions during charging. The SoC estimator provides crucial information on the battery's percentage of charges left, allowing for better planning of the AGV workload. The autonomous charging parameter adjustment enables fully automated AGV charging processes, while IoT data management captures valuable data for analysis and preventive measures. Overall, the battery charging station's flexibility and ease of customization make it ideal for exploring different charging profiles in the future.

Additionally, the study provides a comprehensive evaluation of CC-CV and MSCC charging profiles based on real hardware experimentation, easing users to choose suitable charging profiles for their applications by judging from the actual data generated from the battery charging station itself.

1.7 Outline of the Report

Chapter 1 introduces the project by providing an overview of the battery charging station for AGV, including its purpose and importance. The chapter also discusses the aim, objectives, and problem statement of this project.

Chapter 2 provides a literature review of existing research related to the mechanical aspects of battery charging stations for AGVs and the different charging profiles that can be used. The chapter presents a comprehensive overview of the advantages and disadvantages of different charging profiles.

Chapter 3 outlines the methodology of this project, detailing how the battery charging station was built and how testing was performed. The chapter provides detailed instructions for each stage of the process, highlighting the electronic parts required and the key considerations to be taken into account.

Chapter 4 is divided into two sections. The first section presents the results and discussion of the performance of the battery charging station built. The chapter highlights the key features and functions of the charging station and discussed its performance in detail, including any issues that were encountered during testing. The second section presents the results and discussion of the CC-CV and MSCC charging profiles. The chapter provides a detailed comparison of the two profiles based on the data generated during testing.

Chapter 5 concludes the entire project, stating the findings of this project and its significance. The chapter provides a few recommendations that can be performed on the battery charging station in the future to further improve its performance.

CHAPTER 2

LITERATURE REVIEW

2.1 Introduction

The development of a AGV charging station is divided into two sections which are the mechanical and electrical designs. These sections are crucial and work interconnected with each other. This literature review involves research of various alternatives and considerations that this project can or should adopt in order to build an AGV charging station that can solve the problems discussed in Section 1.3.

2.2 Mechanical Design

2.2.1 Contact and Contactless charging methods

All AGV charger architectures can be divided into contact or contactless chargers. As shown in Figure 2.1, contact chargers are usually performed using extendable electrodes or retractable shields that connect the battery's terminal to the power supply, while contactless chargers involve inductive power transmission, where a magnetic field generated from the power supply induces electricity in the coil in the charging station as shown in Figure 2.2.

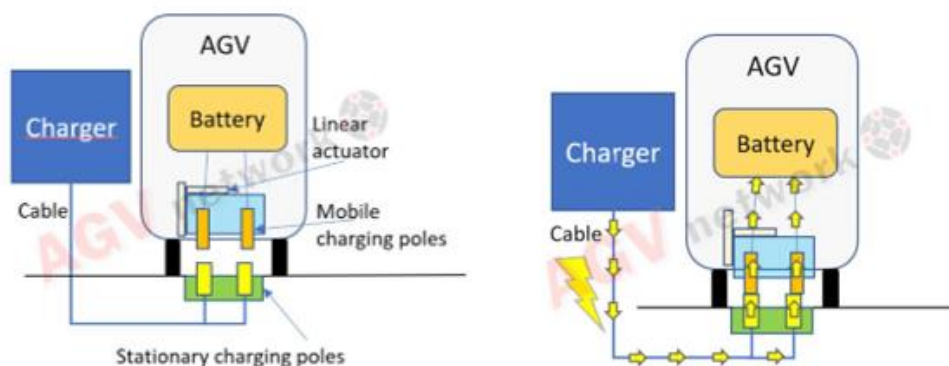


Figure 2.1: Contact charging (Super User, n.d.)

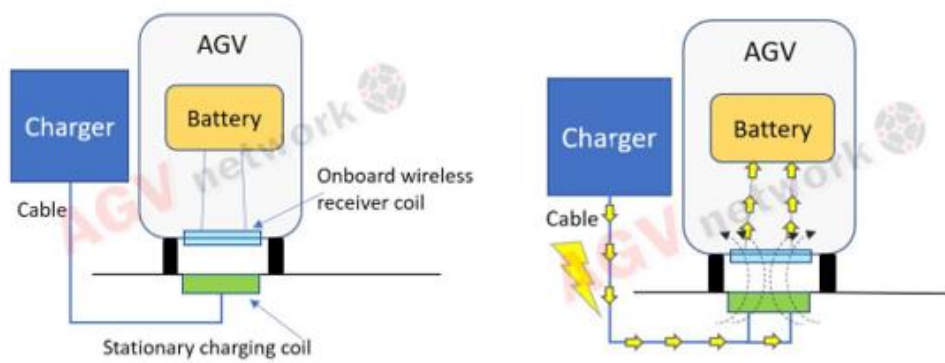


Figure 2.2: Contactless charging (Super User, n.d.)

2.2.2 Comparison between contact and contactless charging

The advantages of contactless charging include its compact size as the main components are coils, which makes it more space-efficient compared to contact charging, which requires extruding contacts, plugs, or sliding mechanisms that would make the charging station larger. Furthermore, contactless charging is practically maintenance-free as there are no mechanical contacts and no moving parts, unlike contact charging. Additionally, contactless charging can supply power to different vehicle sizes and positions, as charging can be done as long as the vehicle is parked below the charging pad as illustrated in Figure 2.3 and Figure 2.4. As a result, AGVs can arrive at the charging station from all directions, making contactless charging more flexible and suitable for "In-Process-Charging," which is a charging strategy that charges the AGV for a short duration while the AGV is waiting for a new mission (Super User, n.d.).

However, contactless charging requires a high initial investment cost compared to contact charging, making it relatively unsuitable for small production factories.

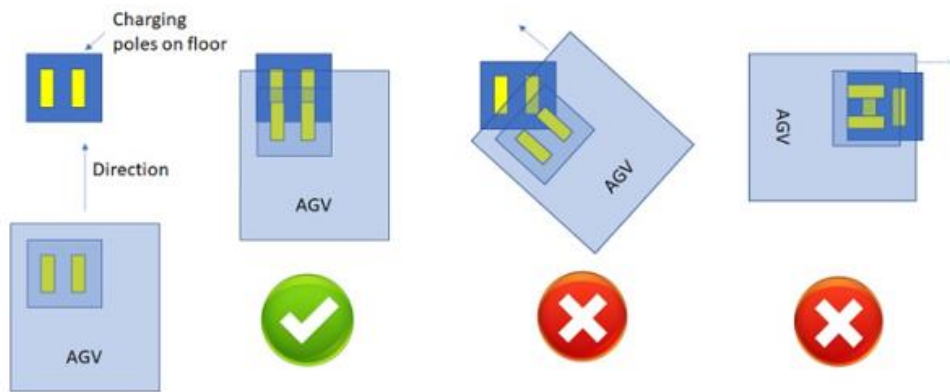


Figure 2.3: Contact charging alignment (Super User, n.d.)

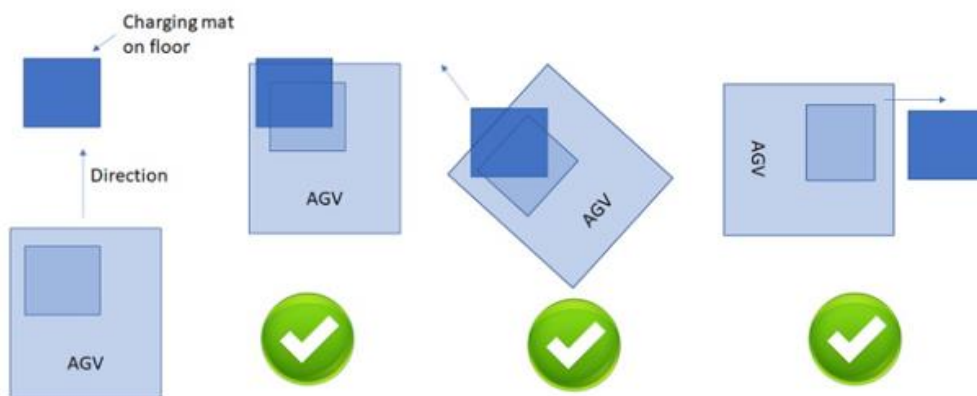


Figure 2.4: Contactless charging alignment (Super User, n.d.)

2.3 Electrical Design

2.3.1 Battery Charger

Figure 2.5 shows the basic battery charger block diagram. Generally, lithium-ion battery chargers consist of a switching mode AC/DC converter to convert AC power from plug to suitable DC power and a DC/DC converter that helps to control the charging profile of the battery.

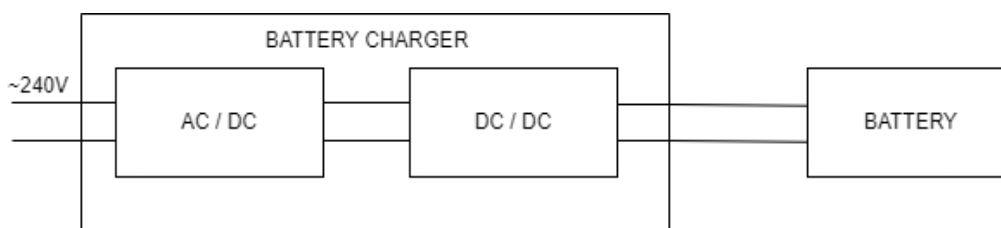


Figure 2.5: Basic battery charger block diagram

2.3.2 AC/DC converter

Most of the switching mode AC/DC converters consist of several similar basic electronics. Figure 2.6 shows the block diagram of the AC/DC converter, the HOT region represents the region with high voltage while the COLD region represents the region with lower voltage. At the HOT REGION (Input side), when AC power is supplied to the converter, it first passes through an EMI filter to eliminate any harmonics present in the input. The AC input is then rectified and filtered to convert it into unregulated DC. The DC source then goes through a power switch, which is controlled by feedback to turn on and off at a high frequency, thereby modifying the DC waveform into AC. The modified AC is then sent into the transformer.

At the COLD REGION (Output side), the transformer steps down the voltage. A small filter is used to smooth and rectify the output. This rectification can be done with a simple filter because the output from the transformer consists of a high-frequency AC waveform.

At the FEEDBACK region, the difference between the output voltage and reference voltage is amplified. An isolator is used to separate the HOT and COLD regions so that any electrical faults in the HOT region do not damage the appliances in the COLD region. The output from the error amplifier changes the PWM driver, which, in turn, changes the frequency of the switch in the HOT REGION (Analog, n.d.). To change the output voltage, the reference voltage connected to the feedback can be increased or decreased. This changes the frequency of the switch turning on and off, which alters the duty cycle of the voltage in the primary circuit. If the duty cycle increases, the output voltage increases, and vice versa.

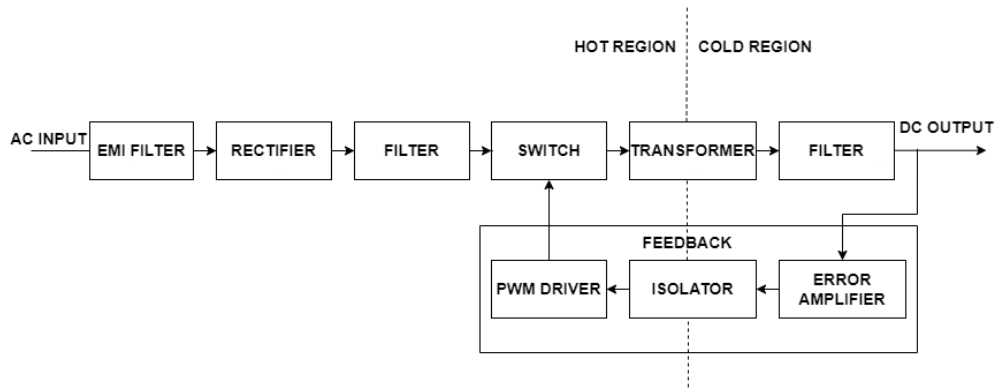


Figure 2.6: Block diagram of switching mode power supply

2.3.3 Examples of AC/DC switching mode power supply

Figure 2.7 shows the configuration of an industrial AC/DC switching mode power supply, DER 453. Referring to the zoomed input region in Figure 2.8, DER 453 uses an additional snubber circuit to protect the switch from transients generated by the transformer. Besides that, zoomed output region shown in Figure 2.9 shows the protection circuit, transformer's output, and output filter which were similar to the switching mode power supply configuration discussed in Figure 2.6 except that an additional protection circuit was added while its feedback loop shown in Figure 2.10 uses an opto-isolator device as the isolator and an auxiliary coil from the transformer's output is used to power the feedback circuits.

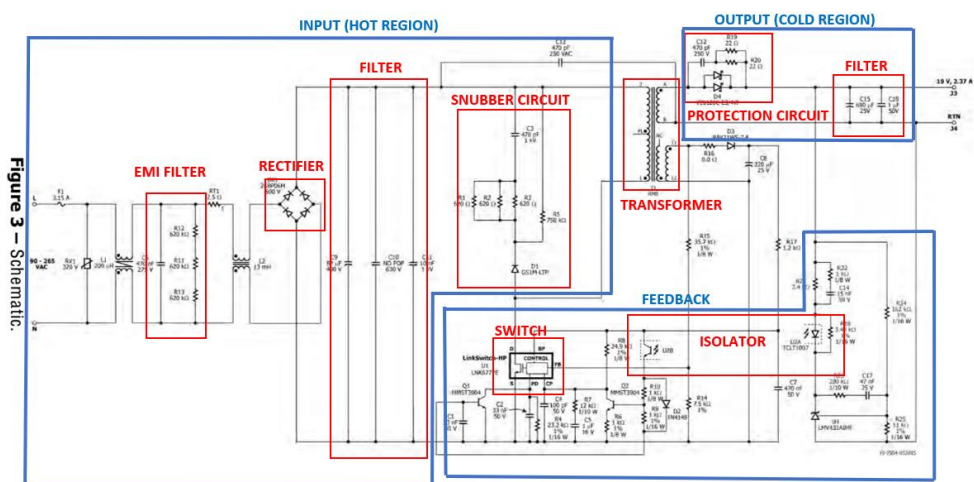


Figure 2.7: DER 453 schematic diagram (Powerint, 2016)

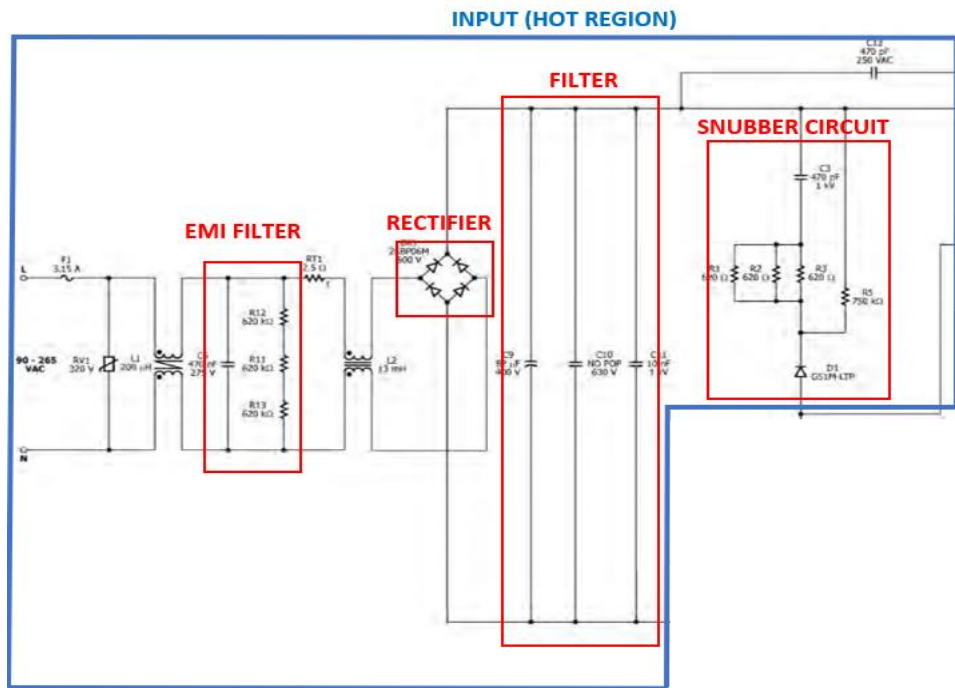


Figure 2.8: DER 453 Zoom in Input region

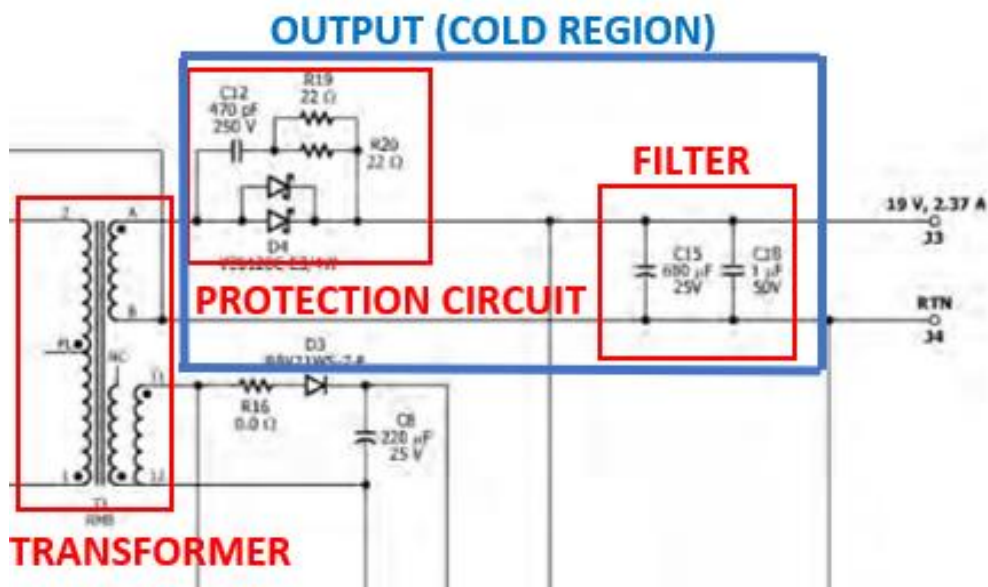


Figure 2.9: DER 453 Zoom in Output region

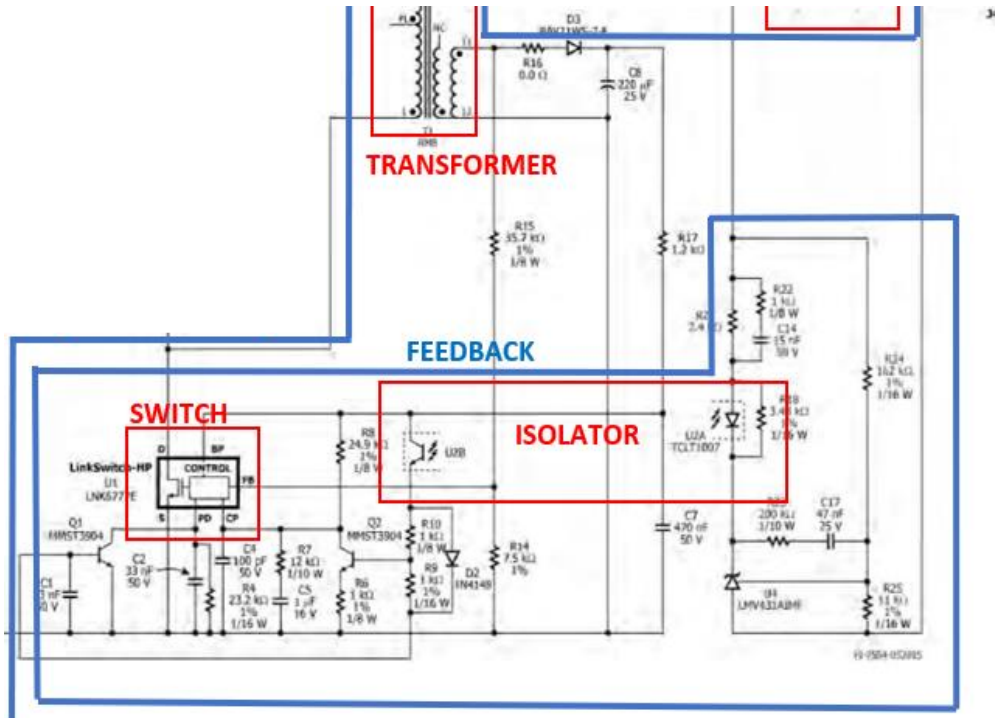
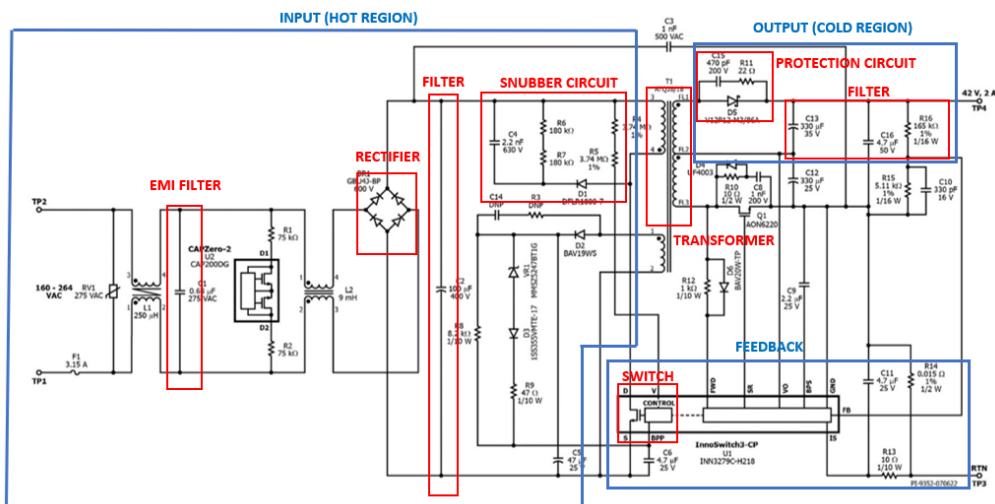


Figure 2.10: DER 453 Zoom in the Feedback loop

Next, Figure 2.11 shows another industrial switching mode power supply, DER 915. The input region shown in Figure 2.12 and output region shown in Figure 2.13 were similar to the input and output region of DER 453. However, referring to Figure 2.14, this switching mode power supply uses an integrated circuit (IC) to control the feedback, this makes the circuit simpler and more organized as compared to DER 453 feedback loop.



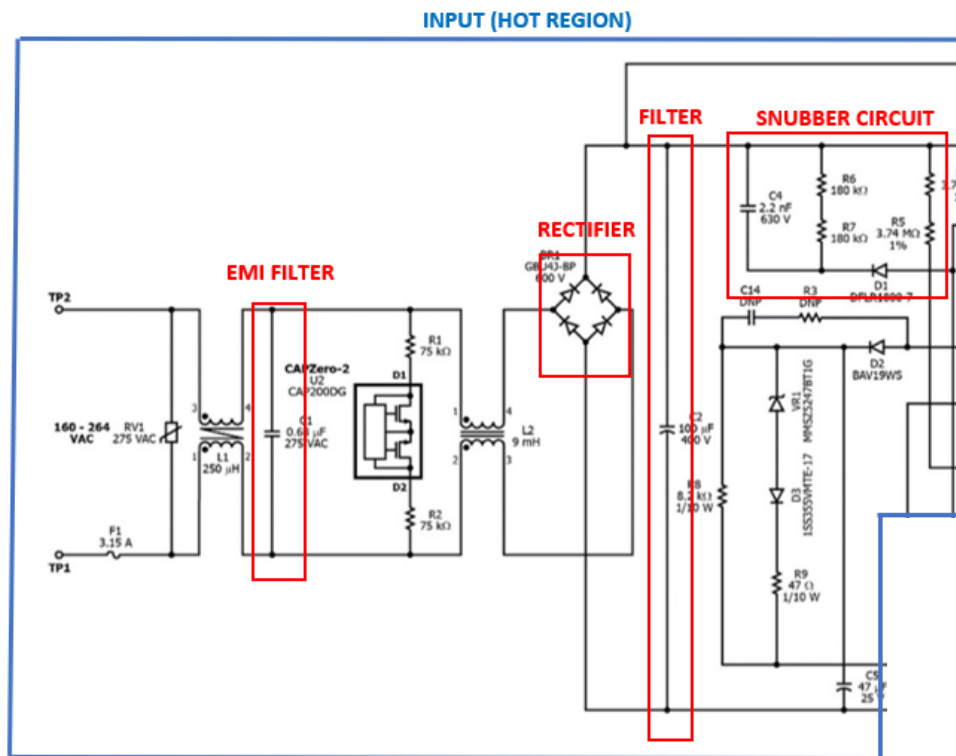


Figure 2.12: DER 915 Zoom in Input region

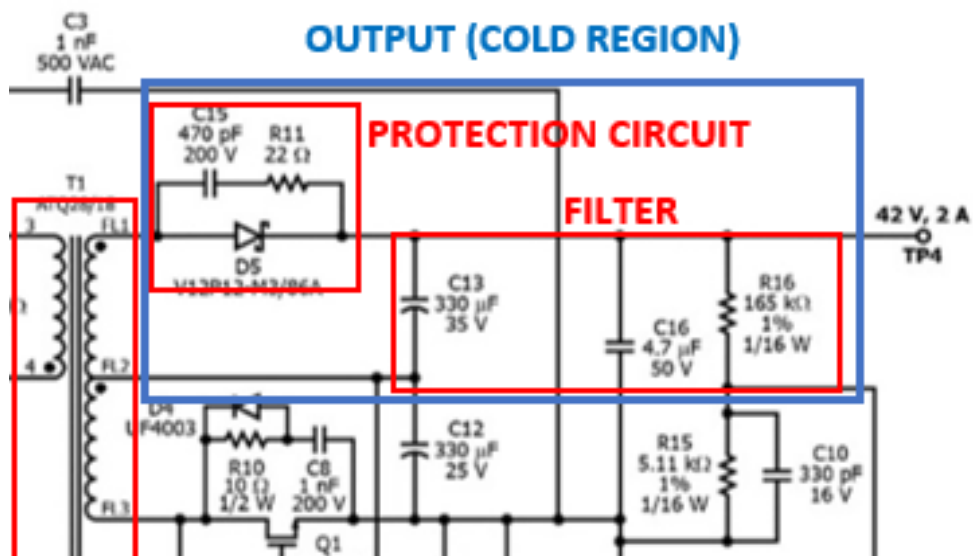


Figure 2.13: DER 915 Zoom in Output region

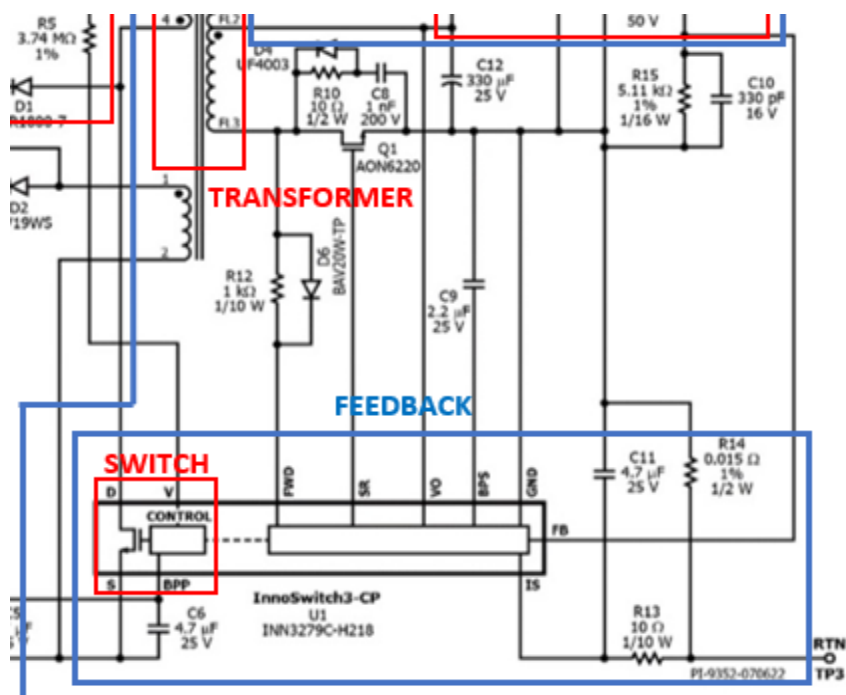


Figure 2.14: DER 915 Zoom in the Feedback loop

2.3.4 DC/DC Converter

In practice, most battery chargers use a current and voltage feedback loop to regulate the charging process of the battery.

As shown in Figure 2.15, the output from both feedback loops is channeled to the buck/buck-boost converter, and the dominant feedback will change the PWM signal or the amount of resistance, altering the voltage or current accordingly. Both feedback errors are channeled to an "OR" logic to allow synchronization between Constant Current and Constant Voltage (Chen and Rincon-Mora, 2006). Additionally, for the voltage feedback loop, the output voltage is measured and compared with the reference voltage value. The error is then amplified and channeled into the buck/buck-boost converter. For the current feedback loop, the output current is controlled by measuring the voltage drop of a resistor connected to the output. The output current is measured from the voltage drop using Ohm's law or by using a transconductor.

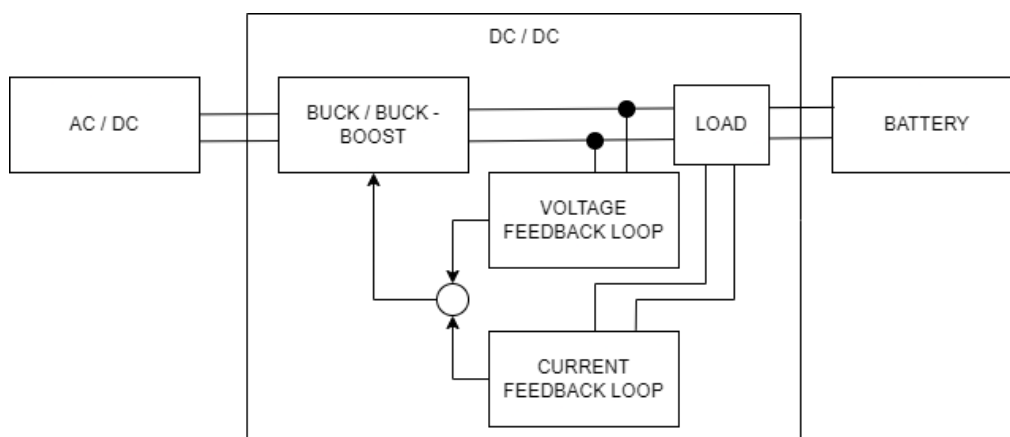


Figure 2.15: DC/DC converter, Dual feedback loop

2.3.5 Example of DC/DC design

Figure 2.16 shows the configuration of the battery charger that performed CC-CV proposed by Chen and Rincon-Mora in 2006. The battery charger uses two feedback loops as discussed in Section 2.3.4. It should be noted that although this design was proposed in 2006, its working concept is still widely used today in battery chargers. The design utilizes both a current and a voltage feedback loop. During the constant current charging mode, the voltage drop across the resistor R_c is directed to a transconductor, which in turn controls the switch M_p . In the constant voltage mode, the voltage flows directly to the switch, which then dominates the switch and transitions the charger from CC to CV mode. The current flow will decrease until it reaches around $0.1C$, and then switch M_{End} will be triggered, stopping the charging process. On the other hand, Figure 2.17 shows a battery charger utilizing the proposed battery charger design, the input side was connected to a switching regulator while the output side was connected to the battery.

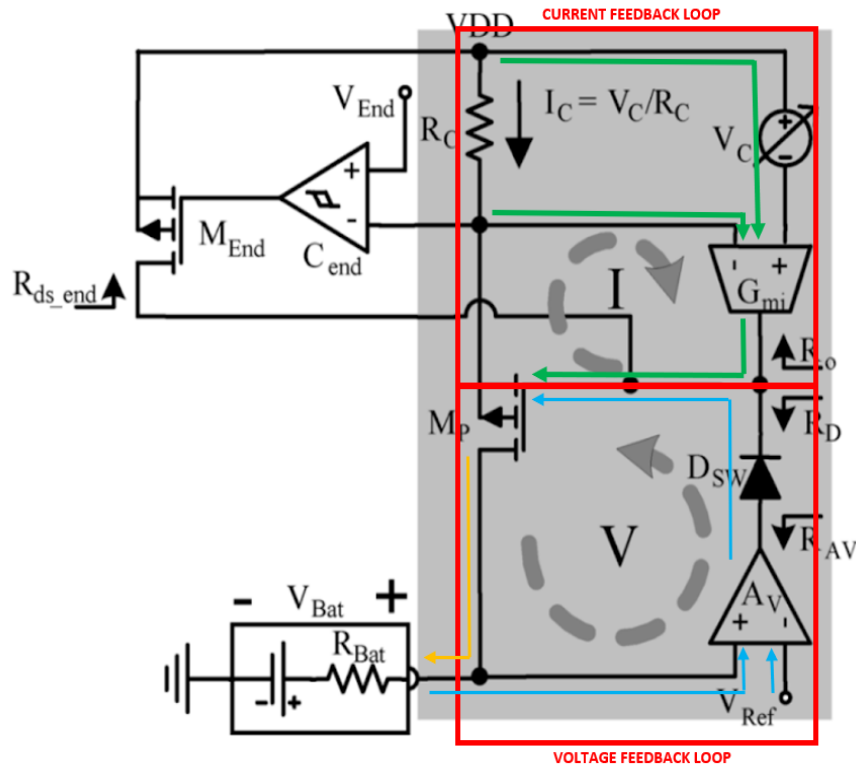


Figure 2.16: Chen and Rincon-Mora, Dual feedback loop design (Chen and Rincon-Mora, 2006)

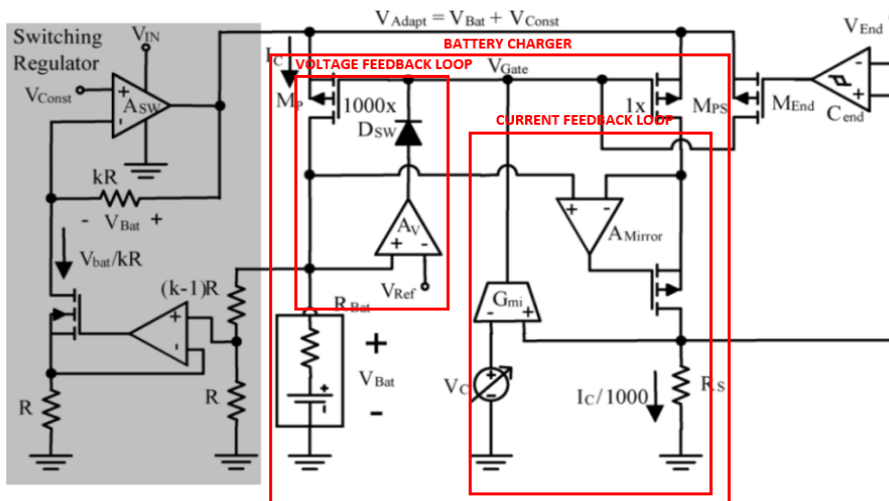


Figure 2.17: Chen and Rincon-Mora, Design application (Chen and Rincon-Mora, 2006)

Figure 2.18 shows the AP4305 schematic. It utilizes the same control mechanism which uses two feedback loops, one for the current feedback loop and one for the voltage feedback loop. The voltage feedback loop is compared

with the internal reference voltage source of 1.21V while the current feedback loop is taking the voltage drop across resistor R_{ss} as the controlled output. Both the output from the feedback loop is connected together and is used to control the optoisolator to change the PWM signal.

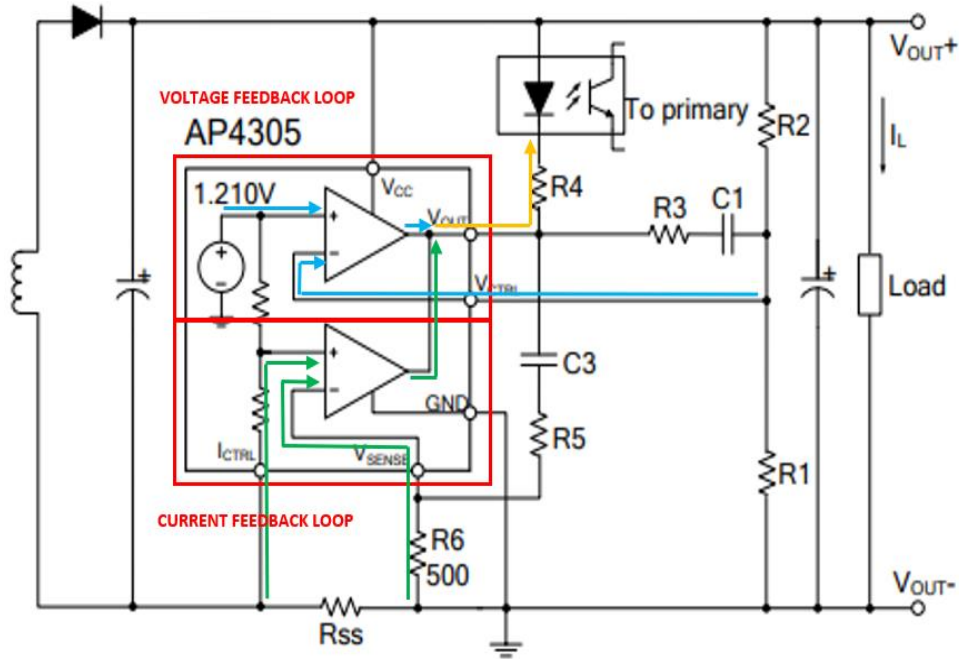


Figure 2.18: AP4305 schematic (DigiKey, 2022)

Figure 2.19 shows the block diagram for MP26085. This design also uses 2 feedback loops in which the outputs are connected together while Figure 2.20 shows the charger being used together with an AC/DC in order to create a complete battery charging system.

2.4.1 Constant voltage(CV) charging

The constant voltage charging algorithm charges the battery with a fixed voltage that is equivalent to the cut-off voltage of the battery. One advantage of CV charging is that the battery charger design is relatively simple. However, the main drawback of CV charging is the long charging time required, as the current flow is very low compared to other charging methods. This long charging time creates persistent underlying pressure in the battery, which can shorten its overall lifespan. (Jha et al., 2022). Figure 2.21 shows the voltage, current, and SoC of the battery against time, the gradient of the SoC was less steep as compared to the gradient of CC-CV charging in Figure 2.23.

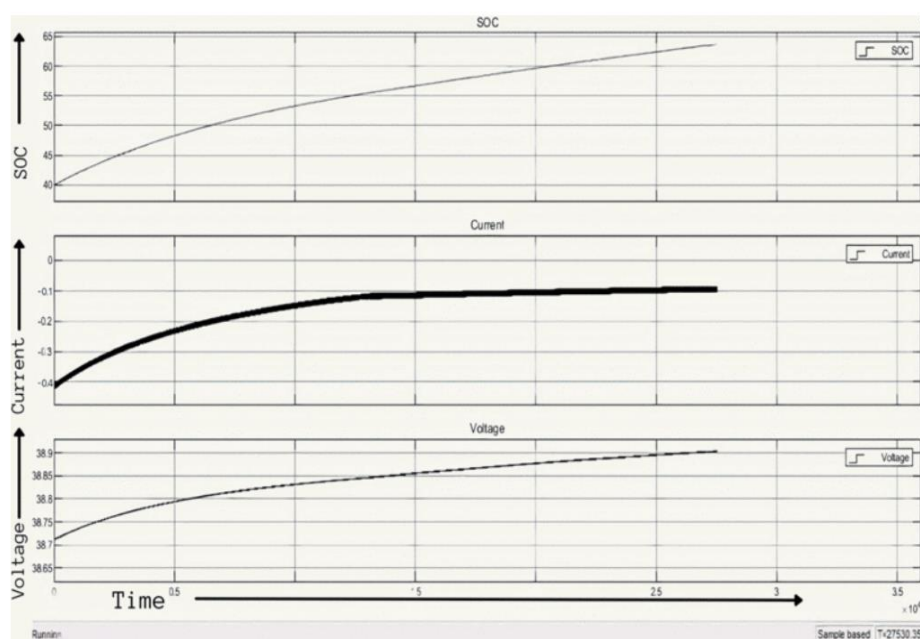


Figure 2.21: CV, Graph of SOC, Current, and Voltage against time (Jha et al., 2022)

2.4.2 Constant current - Constant voltage (CC-CV) charging

As shown in Figure 2.22, the constant current - constant voltage charging algorithm is divided into two modes of operation. The first mode is the constant current mode, in which the battery is charged with a constant current supply while the voltage is continually increased until the cut-off voltage of the battery is reached. Once the voltage reaches the battery's terminal voltage, the charging enters into the second mode of operation, the constant voltage mode. In constant

voltage mode, the battery's cut-off voltage is maintained at a value slightly higher than the emf of the particular battery, causing the current to decrease as the difference between the terminal voltage and emf decreases. When the charging current drops to a certain threshold, typically $0.02C$, the battery is considered fully charged (Jha et al., 2022). The advantages of CC-CV charging are that it charges the battery faster due to the CC operation mode as shown in Figure 2.23, and it does not shorten the battery's life as much as CV charging does.

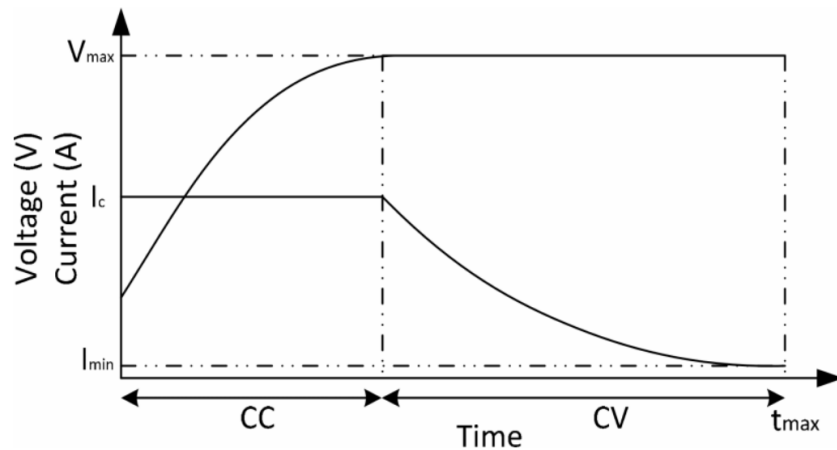


Figure 2.22: CC-CV charging profile (Shen, Tu Vo, and Kapoor, 2012)

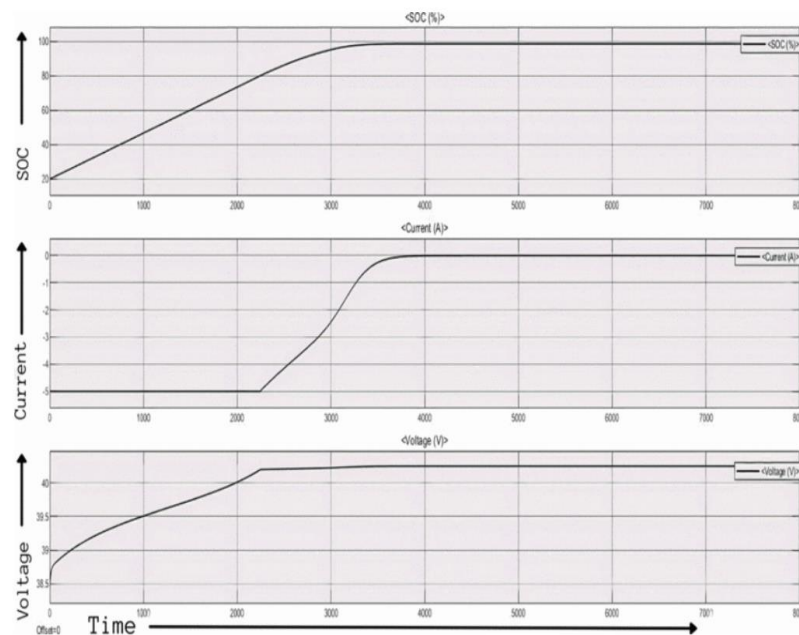


Figure 2.23: CC-CV, Graph of SOC, Current and Voltage against Time (Jha et al., 2022)

2.4.3 Multiple Stage Constant Current (MSCC) charging

In MSCC, multiple different CC modes of charging are used where each current level is lower than the previous current level as shown in Figure 2.24. The algorithm measures a number of parameters of the battery during charging and varies the current levels to charge the battery based on the parameters measured. At each stage, a different current level is injected into the battery. When the battery's voltage reaches its cut-off voltage, the charger changes the current level to the next current level which is lower than the previous current level. This process repeats until the battery reaches the termination criteria (Jha et al., 2022). Just like the charging profile, the current of the battery also increases in stepwise waveform as shown in Figure 2.25.

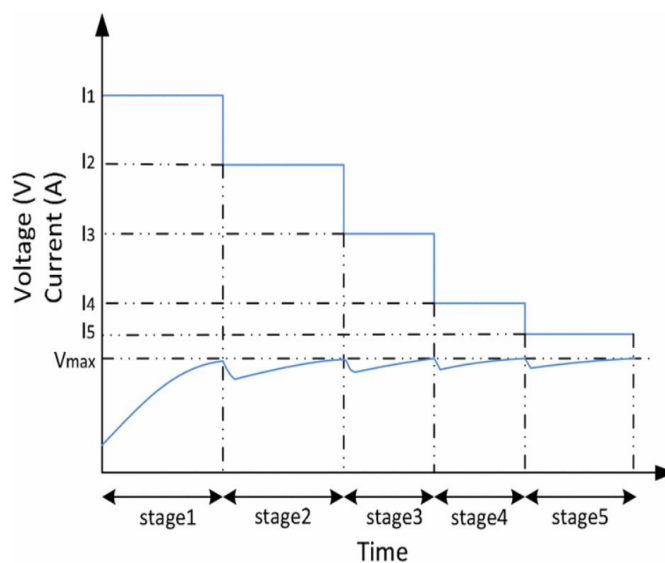


Figure 2.24: MSCC charging profile (Jha et al., 2022)

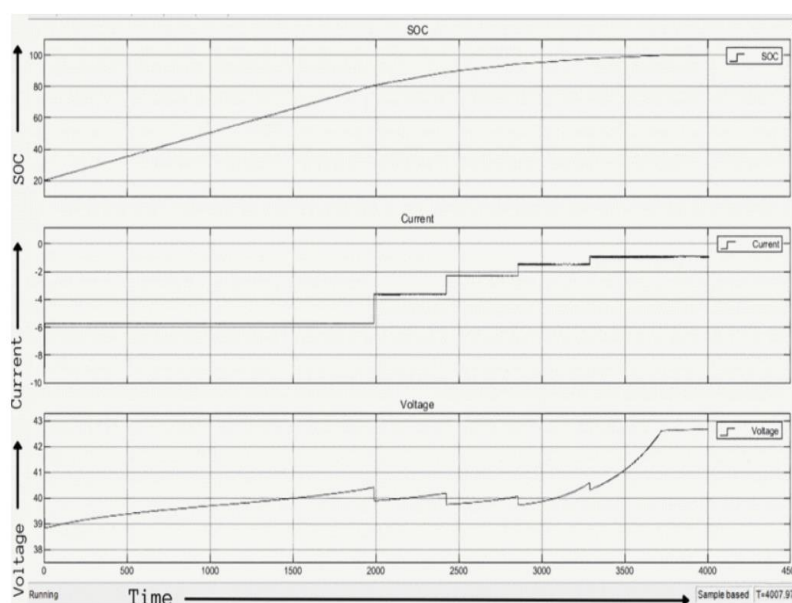


Figure 2.25: MSCC, Graph of SOC, Current and Voltage against Time(Jha et al., 2022)

2.4.4 Comparison between CC-CV and MSCC

Jha et al. (2022) compared the CV, CC-CV, and MSCC charging profiles using MATLAB, and their results showed that the MSCC profile charges faster when the current level is set to the maximum allowable level. Moreover, it does not significantly shorten the battery life compared to CV or CC-CV charging methods due to its fast charging time. The authors also mentioned that implementing MSCC efficiently requires a large amount of data and a study of the charging patterns specific to the battery to find its optimum charging pattern (OCP) is necessary in order for MSCC to work efficiently. This makes it labor-intensive, time-consuming, and significantly increases implementation costs. However, Jha et al.'s findings were based on simulations and may yield different results in actual testing.

In contrast, Li Jiang et al. (2020) used the Taguchi method to find the OCP for MSCC. Their findings showed that under the OCP, MSCC actually has approximately similar charging speed to CC-CV, which is different from Jha et al.'s findings. This is because, Li Jiang et al. claimed that MSCC charging current is a trade-off between multiple indicators such as charging efficiency, temperature rise, and battery health. The OCP that they found (5.4A – 4.1A – 2.8A – 1.6A – 0.6A) resulted in the least temperature rise and higher charging efficiency. Additionally, an article by Renhotec Technology Electronics (2022)

supports Li Jiang et al.'s claim that just increasing the charging current will not necessarily result in faster charging time. This is because higher current causes an increase in the polarization of the battery, which causes the battery to reach the cut-off voltage quicker. Despite reaching the cut-off voltage, the battery is not fully charged and can only be depolarized by a slow constant voltage or lower charging current to continue charging. Therefore, it can be concluded that MSCC does not necessarily charge the battery faster than CC-CV. However, all three papers claim that MSCC is better than CC-CV in terms of maintaining battery health.

2.5 Summary

In summary, for the mechanical design consideration, contact charging is chosen over contactless charging due to the high initial investment of the latter. The charger will be used to perform CC-CV and MSCC charging profiles, where CC-CV will charge at 1C and terminate at 0.2C, and MSCC will follow the OCP found by Li Jiang, et al., which is 5.4A – 4.1A – 2.8A – 1.6A – 0.6A.

CHAPTER 3

METHODOLOGY AND WORK PLAN

3.1 Introduction

The current design of the AGV charging station utilizes the IMAX B6 battery charger, which employs the CC-CV charging profile. The design requires users to remove the AGV battery and manually plug it into the battery charger. The IMAX B6 supports charging, discharging, storage, and balance charging for various battery types, and the voltage rating for each battery type is fixed while the current limit is adjustable. The battery charger's LCD display shows the voltage of each battery during the charging process, providing a safe and efficient charging experience.

However, the IMAX B6 charger is not automated and can only perform conventional CC-CV charging. Additionally, the current charger only displays information on the charger itself, which can be challenging in industrial settings where operators need to monitor multiple AGVs and battery chargers. Not to mention, it also lacks functions such as SoC estimation and data management. The new charging station design will address these issues.

3.2 Prototype design

Figure 3.1 shows the block diagram for the proposed prototype.

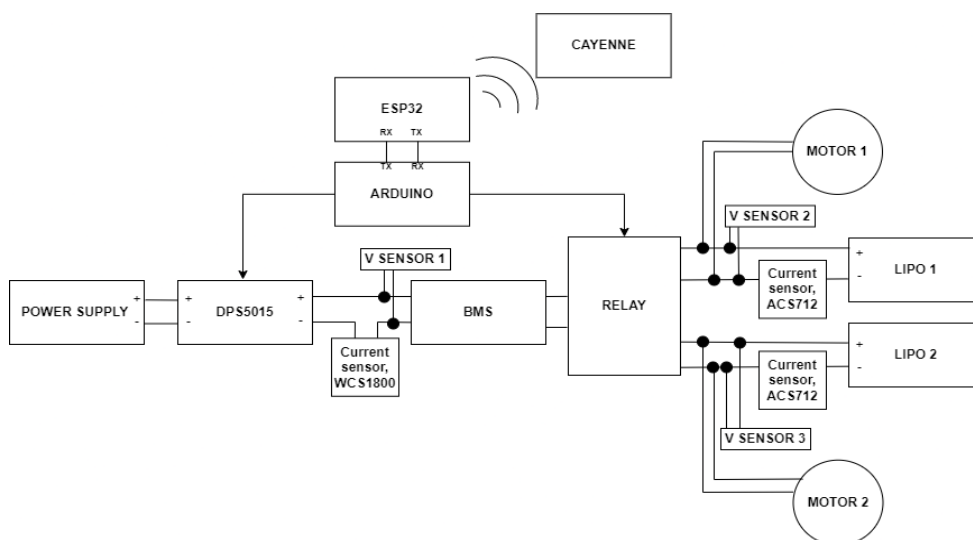


Figure 3.1: Complete system prototype

3.2.1 Prototype's components

The power supply selected for the new charging station is an AC/DC switching mode power supply with an output voltage of 24V, a current rating of 6.5A, and a total power output of 156W. This power supply is capable of converting the alternating current (AC) from a standard 240V plug into a stable direct current (DC) that can be used to charge the AGV's battery. By directly connecting the power station to the plug using this power supply, the charging process will be more efficient and easier to manage. Additionally, the high current rating and total power output of the power supply will allow faster charging times and more reliable performance.

The DPS5015 is a DC/DC converter that utilizes integrated circuits (ICs) to control the charging profile. It is capable of performing CC-CV charging profiles. The original DPS5015 model includes a separate control panel that allows the user to manually adjust the charging current and voltage, as well as start and stop the charging process.

Hall effect current sensors are used to detect the charging and discharging current. They are chosen because the charging current is very high (5.4A), and hall effect sensors, which do not suffer power losses, are more suitable for this application. Moreover, since the measuring circuit is isolated, it provides additional protection to the microcontroller if electrical faults were to occur. The current measured will be used in coulomb counting for SoC estimation.

In order to detect the charging voltage and the voltage of the battery, a voltage sensor module has been selected. The maximum voltage of the entire circuit under normal operation is 12.6V, and the voltage sensor module that has been chosen can detect a maximum voltage of 25V, making it well-suited for this application.

A passive 3-cell BMS is used to provide balanced charging to the battery, ensuring that all three cells are charged simultaneously.

Two sets of optoisolated relay modules are used to connect the battery charger to the battery when it is charging and disconnect it when it is not charging. In addition, two relays are used, one for each battery pack, so that the battery charger can switch to charge the other battery when the first battery has

been fully charged. This mechanism allows one battery charger to charge two battery packs (one at a time).

The Arduino controls all the charging circuit operations, including the automation of the DPS5015, SoC estimation, and sensor readings. Every six seconds, the Arduino will transfer the charging data, such as voltage, current, and SoC, to the ESP32 via UART (Universal Asynchronous Receiver Transmitter) communication. The purpose of using the ESP32 is to establish a WiFi connection and send data to a web server. Upon receiving the data, ESP32 will send it to Cayenne for storage and monitoring.

Cayenne is a web server that is specially designed for IoT applications. Cayenne will receive the data from ESP32 and then display and store it in cloud. The battery used to test the charger is similar to the one used in the reference AGV, which is a 3-cell LiPo battery.

3.2.2 Building prototype

This section will focus on the prototype building process, which involves the use of individual components such as the voltage sensor, current sensor, and BMS. It will also cover modifications made to DPS5015. Additionally, it will discuss how the components were combined together through serial communication, how communication was established between the ESP32 and Cayenne, and how SoC estimation was done. Please note that minor details such as wiring and relay setup will not be discussed in this section as these aspects are not the primary focus of this project.

3.2.3 BMS

The passive 3-cell BMS (Figure 3.2) used in the project had four ports: 0V, 4.2V, 8.4V, and 12.6V, that needed to be connected to the 4 BMS ports of the LiPo battery. Firstly, the BMS port of the LiPo battery was identified as shown in Figure 3.3, the thicker red and black wire represents 12.6V and 0V respectively while the thinner black wire represents 8.4V and 4.2V. Next, a XH2.54 4P female connector (Figure 3.5) was soldered to the BMS, according to its respective port voltage. During the charging process, the female connector from

the BMS must be connected to the battery's male connector (Figure 3.4) in order to perform balance charging.

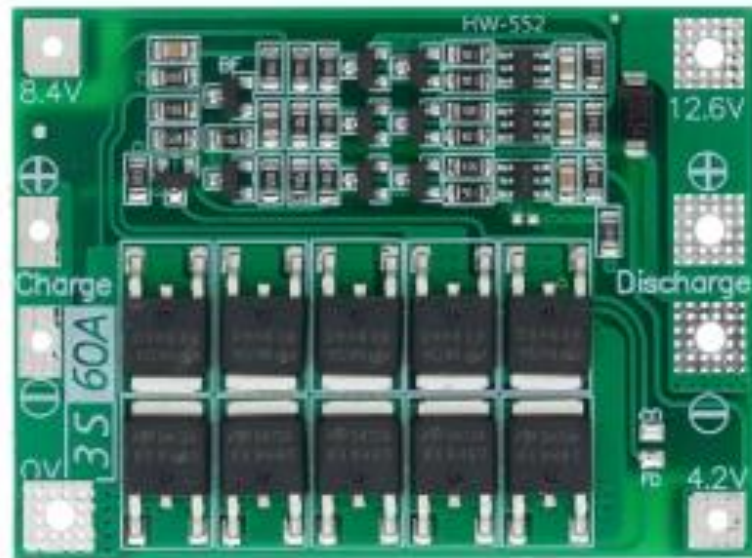


Figure 3.2: 3 - cell BMS



Figure 3.3: LiPo battery BMS port voltage



Figure 3.4: XH 2.54 4P male connector

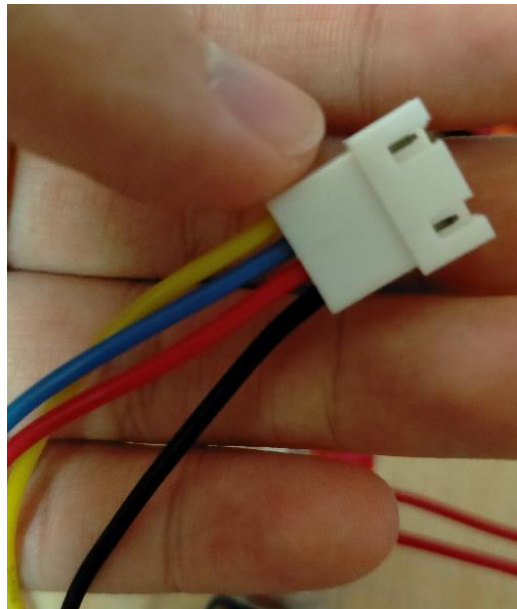


Figure 3.5: XH 2.54 4P female connector

3.2.4 Voltage sensor & Current sensor

The voltage sensor can detect voltages up to 25V and then step them down by a factor of 5 to output 5V. This 5V signal is channeled to the Arduino as an analog input, which is then converted to a digital value by dividing it by 2^{10} bits. This digital value is then multiplied by 5 to obtain the actual voltage measurement.

The ACS712 current sensor outputs voltage in analog form, which includes the voltage increment caused by the measured current as well as half of the source voltage supplied to the sensor. The output voltage is then divided by the sensor's standard sensitivity value, which is 0.1V/A for a 20A sensor, in order to obtain the final output current.

3.2.5 Modify DPS5015

The DPS5015 charging station is equipped with a control panel that allows users to manually adjust the charging current and voltage, and start/stop the charging process. However, the charging process is not automated, and therefore, the DPS5015 must be modified to work with an Arduino in order to automate the charging process.

The control panel of the DPS5015 is connected to the main charger through two 8-pin wire connectors. As shown in Figure 3.7, one set of the 8-wire connector is used to control the LCD screen, while the other set is used to control the buttons on the DPS5015.

To modify the DPS5015 for Arduino control, the pair of wires that control the DPS5015 buttons were probed using a multimeter to identify the wire connected to each button as shown in Figure 3.6. Next, it was found that initially each wire was set to HIGH (3.3v), when a button on the control panel was pressed, it pulled the line to low (0v). Therefore, to control the DPS5015 using an Arduino, the wire from the control panel was extended to Arduino as shown in Figure 3.8. Arduino would pull the line to low (0v) when a button press was required. This way, when the DPS5015 detected the low signal, it would assume that a button had been pressed.

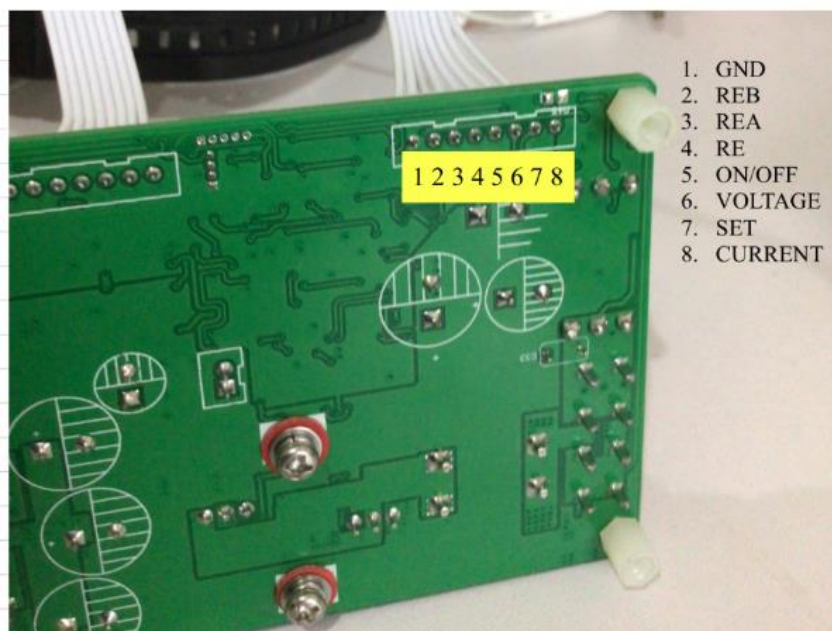


Figure 3.6: Functions corresponding to the 8-pin wire connectors

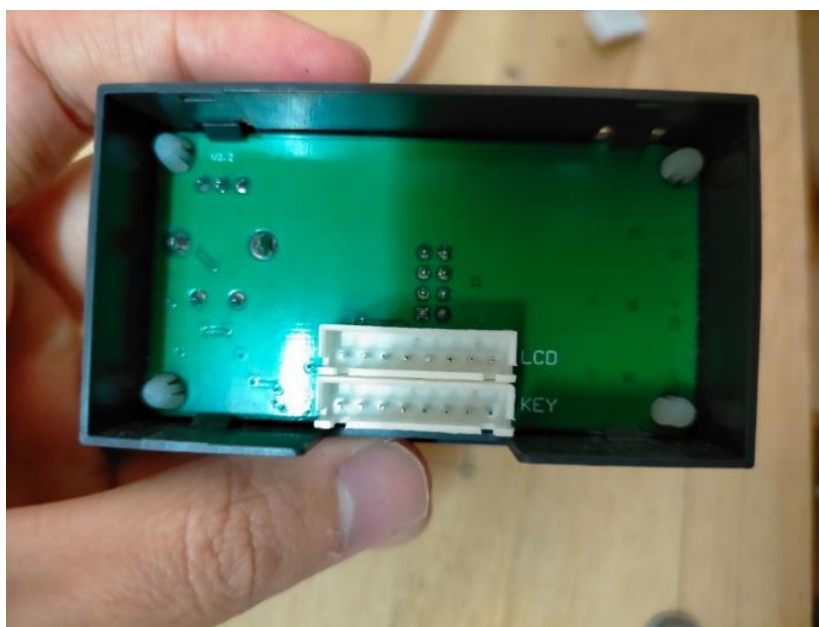


Figure 3.7: DPS5015 control panel

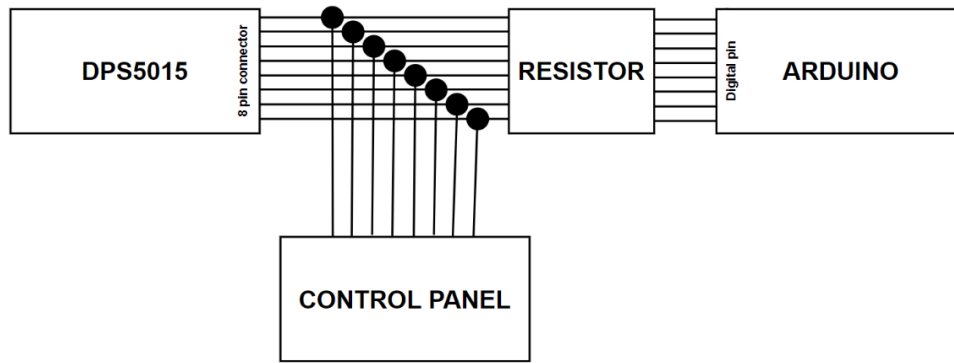


Figure 3.8: Block diagram for Arduino to DPS5015's connection

3.2.6 SoC estimation

The coulomb counting method was used to estimate the SoC of the battery. This method followed the concept of measuring the current flowing into and out of the battery and using it to calculate the amount of charge left in the battery as illustrated in Figure 3.9 (PowerTech, n.d.) while Equation (3.1) is used to calculate the SoC.

$$SoC (\%) = \frac{Current\ capacity\ (Ah) + Current\ (Ah)}{Battery\ capacity\ (Ah)} \times 100\% \quad (3.1)$$

To use this method, the output of the current sensor was converted from amperes (A) to ampere-hours (Ah) by dividing it by 3600s. For example, assume the charging current is 3A while the battery capacity is 3.0Ah:

$$Current = 3A$$

$$Current\ (Ah) = \frac{3A}{3600\ h} = 8.33 \times 10^{-4} Ah$$

The initial SoC before charging is:

$$SoC (\%) = \frac{0.3Ah}{3.0Ah} \times 100\% = 10.00\%$$

The increase in SoC after charging at 3A for one second is:

$$SoC (\%) = \frac{0.3Ah + 8.33 \times 10^{-4} Ah}{3.0Ah} \times 100\% \approx 10.03\%$$

This process is repeated continuously every second to estimate the SoC value.

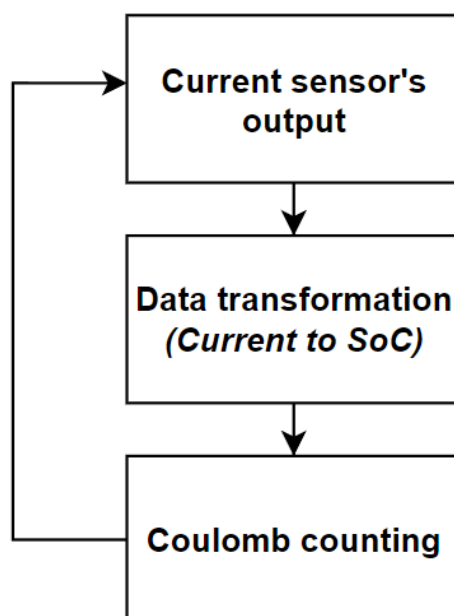


Figure 3.9: SoC estimation

3.2.7 UART communication between Arduino and ESP32

Data such as charging voltage, charging current, SOC, discharging voltage, and discharging current were transferred from Arduino to ESP32 via UART communication. The RX pin of the Arduino was connected to the TX pin of the ESP32. Since Arduino used 5V while ESP32 used 3.3V, the TX pin of the Arduino needed to be connected to a voltage divider circuit before connecting to the RX pin of the ESP32. The voltage divider will reduce the voltage to 3.3V which is safer for ESP32 operation (Life Hacker, n.d.).

The data was transferred when Arduino executed the function "Serial.print()". In order to make the data transfer more efficient, instead of sending the data one by one, the data was converted from float to string type and then all of them were combined together with a reference, 't', between them. This way, Arduino only had to send all the data once, and it also allowed all the data to be updated simultaneously. When ESP32 received the data, it read the data until the reference, 't', and when it reached the reference character, it stopped and stored the data into an array. The process continues until all the variable has been stored into their respective array, then the array was combined into a string and then converted back into float.

3.2.8 Communicating with Cayenne

To send data to Cayenne, the ESP32 needed to insert the username, password, and client ID of the Cayenne server into the code (Figure 3.11), those information were obtained from the Cayenne website as shown in Figure 3.10. After the connection was established, data was sent to Cayenne using the “Cayenne.virtualWrite(channel, data)” function.

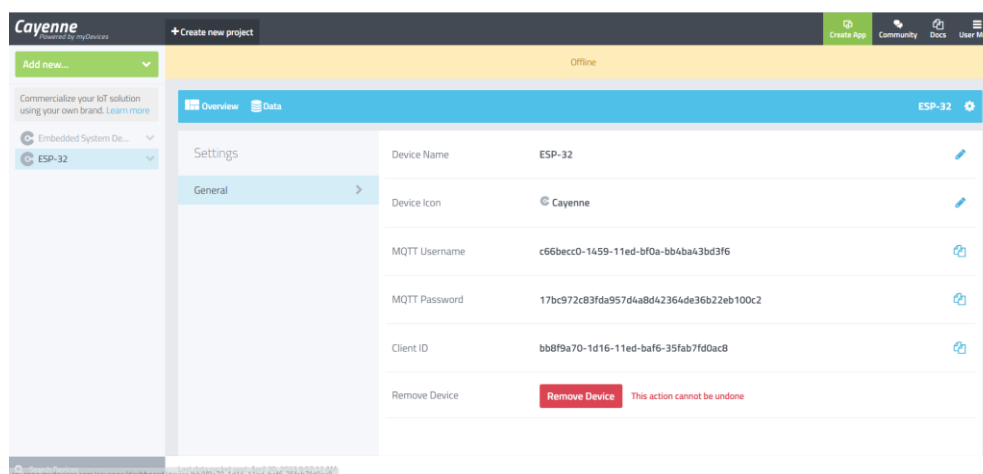


Figure 3.10: Cayenne dashboard

```
char username[] = "c66becc0-1459-11ed-bf0a-bb4ba43bd3f6";
char password[] = "17bc972c83fda957d4a8d42364de36b22eb100c2";
char clientID[] = "bb8f9a70-1d16-11ed-baf6-35fab7fd0ac8";
```

Figure 3.11: Coding to establish connection with Cayenne

3.3 Flowchart for charger operation

The flowchart for the charging operation was shown in Figure 3.12. Initial conditions of the charging were: AC/DC was connected to the plug and switched on, DPS5015 was powered on, the battery was connected to the charging circuit, and ESP32 was connected to WiFi.

Firstly, the charging operation started when the button was pressed. When the button was pressed, Arduino adjusts the DPS5015 charging current according to the preset value while the charging voltage remained the same at 12.60V. Once adjusted, Arduino switched on relay 1 or relay 2 (depending on

which battery is being charged) to connect the charger to the battery, then DPS5015 starts the charging process.

Next, Arduino checked whether the charging termination criteria were met. There were 2 charging termination criteria: the button was released and the charging completion. If either of these two conditions was met, DPS5015 will stop the charging process and disconnects the connection between the charger and battery by switching off the relay. Then it switched to charging the other battery. If neither of the charging termination criteria were met, Arduino will check the MSCC charging current. If the charging current level needs to be adjusted, it will perform current adjustment.

If the current level is correct, the charger will detect the charging voltage and current via sensors and then perform SoC estimation. The SoC estimation will be updated every second. After every 6 seconds of operation, Arduino will send the charging data (voltage, current, SoC) to ESP32 via UART. ESP32 will receive the data and then transfer it to Cayenne where the data was displayed and stored.

When charging with the MSCC profile, Arduino will check whether the charging current had dropped to more than 0.03A of its initial value. If it had dropped to more than 0.03A, it will trigger DPS5015 to change the current level injected into the battery. This operation will continue until the termination criteria was met where it will stop the charging process.

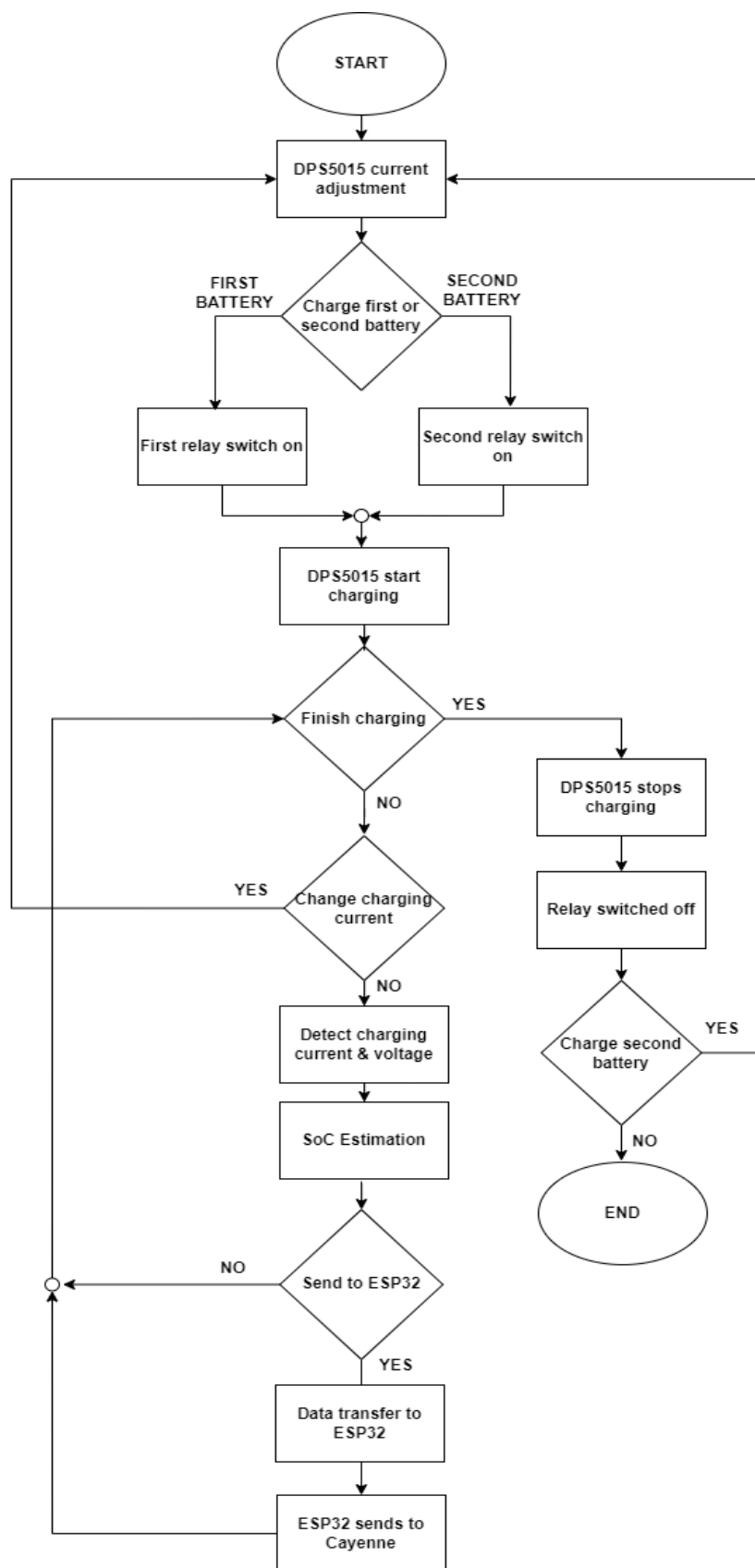


Figure 3.12: Charging operation

3.4 Using the charger to perform CC-CV and MSCC charging

The charger was capable of performing the CC-CV profile without any modifications. However, for MSCC charging, the current had to be adjusted during the process since different current levels were injected into the battery. To determine when to change the current level, Arduino controlled the DPS5015 and adjusts the current level by setting the switching parameter in Arduino. Once the switching parameter was reached, the current would change automatically. The algorithm used to change the current involved a sequence of operations. First, the CURRENT button was pressed to enter the current edit mode, then the RE (rotary encoder) button was pressed to select decimal places. The charging current was then reduced to 0A by twisting the rotary encoder B (REB) and increased to the preset current level by twisting the rotary encoder A (REA). Finally, the CURRENT button was pressed again to exit the current edit mode.

3.5 Testing the charger

In order to test the functions of the battery charging station for AGV, both CC-CV and MSCC charging algorithms were used with termination criteria set at 0.2c (0.6A) and 5 different charging current levels: 5.4A - 4.1A - 2.8A - 1.6A - 0.6A. Additionally, a simple motor discharge circuit was built for testing purposes which consisted of two DC motors, two motor drivers, and an Arduino board. This discharge circuit was used to partially discharge the battery, which was then recharged using the charger in order to test the accuracy of the soc estimation.

3.6 Gantt Chart

As shown in Figure 3.13, Final Year Project 1 involves understanding the project requirements, findings literature review, and doing minor testing on the prototype individually. While Final Year Project 2 consists mainly of building, troubleshooting, and fine tuning the complete prototype as shown in Figure 3.14.

No.	Project Activities	Planned Completion Date	Weeks																
			W1	W2	W3	W4	W5	W6	W7	W8	W9	W10	W11	W12	W13	W14	W15	W16	W17
1.	Understanding project requirement & project planning	2022-06-24	█	█															
2.	Literature review	2022-07-29		█	█	█	█	█	█										
3.	Implementation on methodology & electronics used	2022-07-22			█	█	█	█											
4.	Preliminary testing & investigation	2022-08-12					█	█	█	█	█								
5.	Circuit designing	2022-08-26								█	█	█	█						
6.	Report writing & presentation	2022-09-16											█	█	█	█			
7.	Search for suitable components for building the charging station.	2022-10-29	█	█															
8.	Study and test the battery charger(AC/DC, DC/DC) and Battery Management System(BMS) separately.	2022-12-03			█	█	█	█											
9.	Study and test the communication methods for the controller	2022-12-10							█										
10.	Finalized the components needed in building prototype.	2023-02-04	█																
11.	Combine and test the battery charger(AC/DC, DC/DC) and Battery Management System(BMS).	2023-02-25		█	█	█	█												
12.	Connecting communication lines to controller and code its operation.	2023-03-25					█	█	█	█									
13.	Troubleshooting(if any), fine tuning and documentation.	2023-04-01								█									
14.	Final report, presentation and poster.	2023-05-06										█	█	█	█	█			

Figure 3.13: Gantt Chart for FYP 1

No.	Project Activities	Planned Completion Date	Weeks																
			W1	W2	W3	W4	W5	W6	W7	W8	W9	W10	W11	W12	W13	W14	W15	W16	W17
1.	- Tuning of sensor - Integration of electrical system and testing	2023-02-25	█	█	█	█													
2.	- Designing and building mechanical structures. - Integrating mechanical structure with electrical system.	2023-03-18					█	█	█										
3.	- Full prototype testing and troubleshooting - Result gathering	2023-04-01							█	█									
4.	- Report writing	2023-04-15									█	█							
5.	- Creating poster - Final year project presentation	2023-05-06											█	█	█	█			

Figure 3.14: Gantt Chart for FYP 2

3.7 Summary

The design of the AGV charging station was capable of addressing all the problems mentioned by introducing new functions, such as IoT data management, autonomous charging parameter adjustment, MSCC and CC-CV charging algorithms, and SoC estimation. The DPS5015 was modified to enable autonomous charging parameter adjustment, which was a crucial function for performing MSCC charging profiles. Additionally, ESP32 with WiFi connectivity was used for IoT data management, allowing data to be stored on the cloud. Finally, the SoC estimation function was achieved by receiving the output from the current sensor and combining them every second.

CHAPTER 4

RESULTS AND DISCUSSION

4.1 Introduction

The result and discussion will be divided into two sections. In the first section, the functions of the battery charging circuit will be discussed and the performance of the SoC estimator will be evaluated. In the second section, the battery charging station built will be used to charge the LiPo battery using CC-CV profiles and MSCC profiles. The result from the two profiles will be evaluated and discussed.

4.2 Part 1 Result: Prototype

4.2.1 Battery charging station hardware

Figure 4.1 shows the completed battery charging station's prototype while Figure 4.2 and Figure 4.3 shows the zoomed view of the prototype.

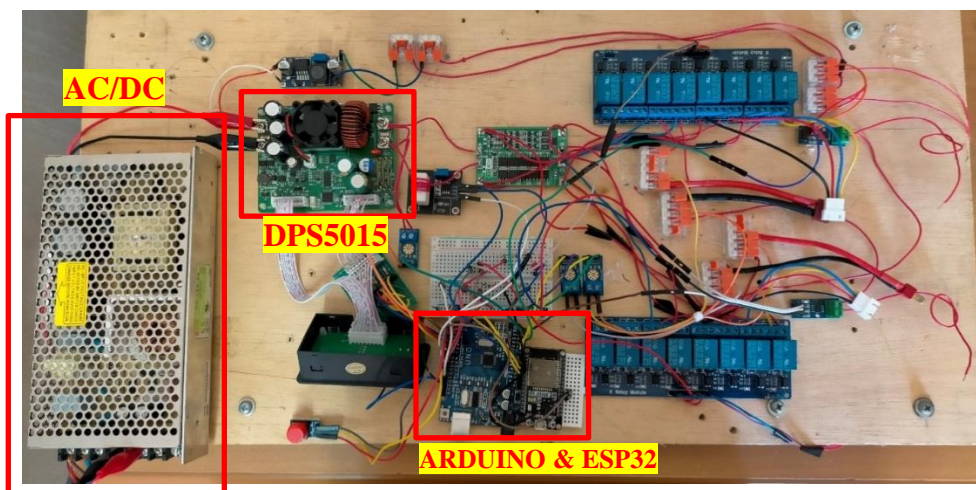


Figure 4.1: Charging station prototype

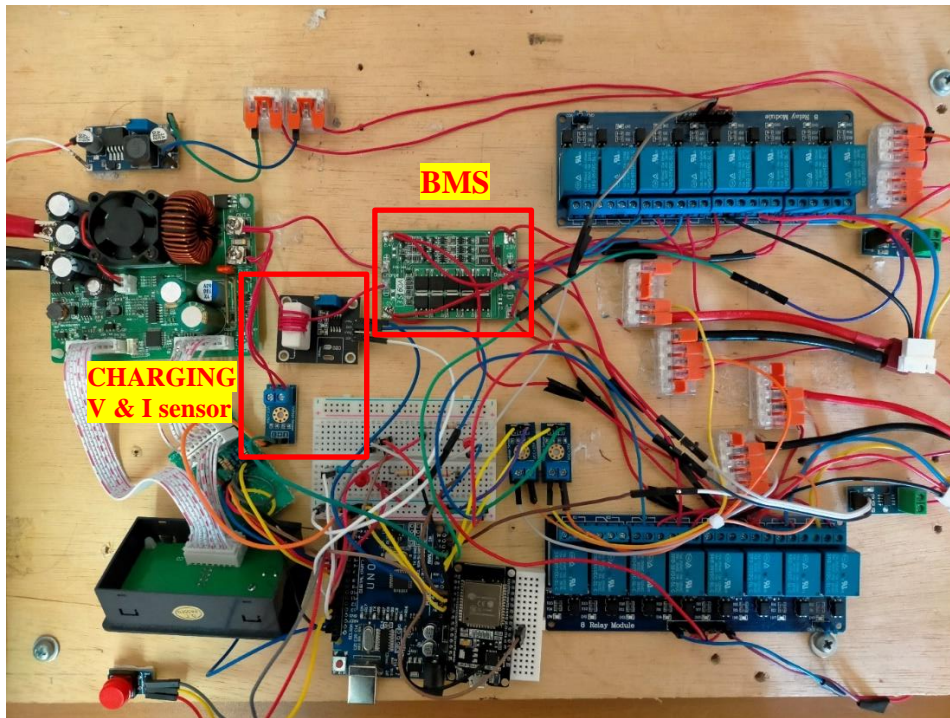


Figure 4.2: Charging station prototype zoom view

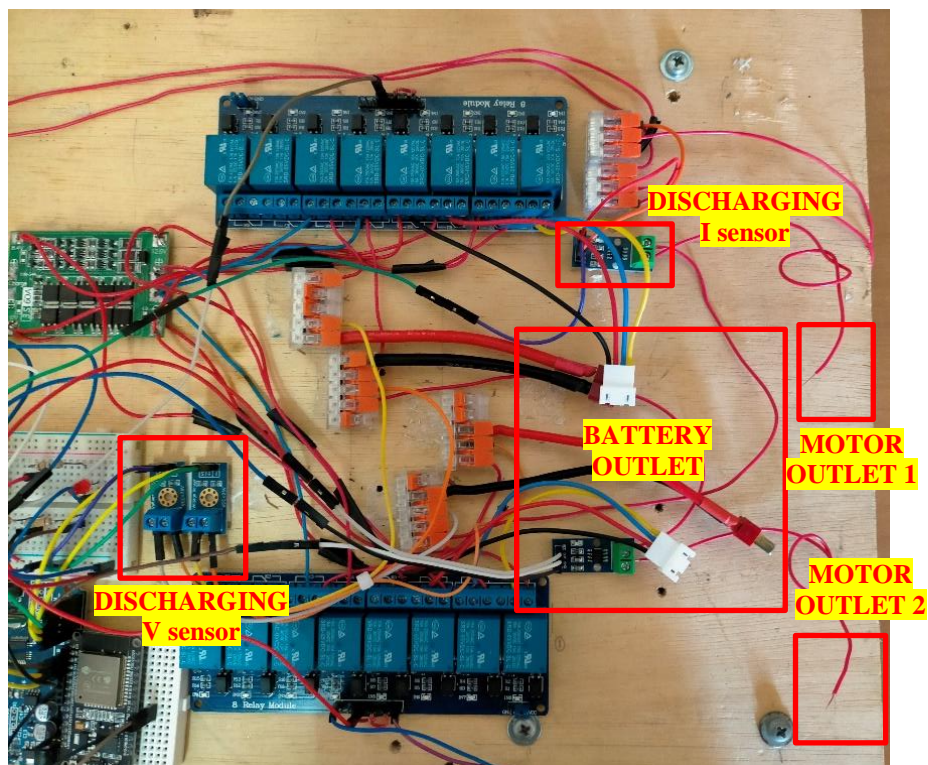


Figure 4.3: Charging station prototype zoom view

4.2.2 IoT data management

Figure 4.4 shows Cayenne's data storage configuration consisting of timestamp, channel, sensor ID, and value while Figure 4.5 shows Cayenne's data visualization function.

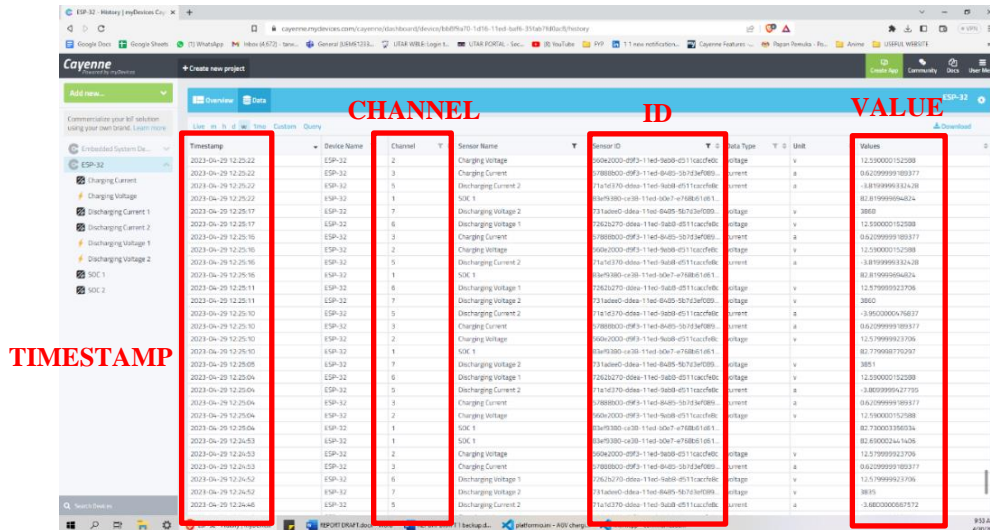


Figure 4.4: Cayenne's data storage

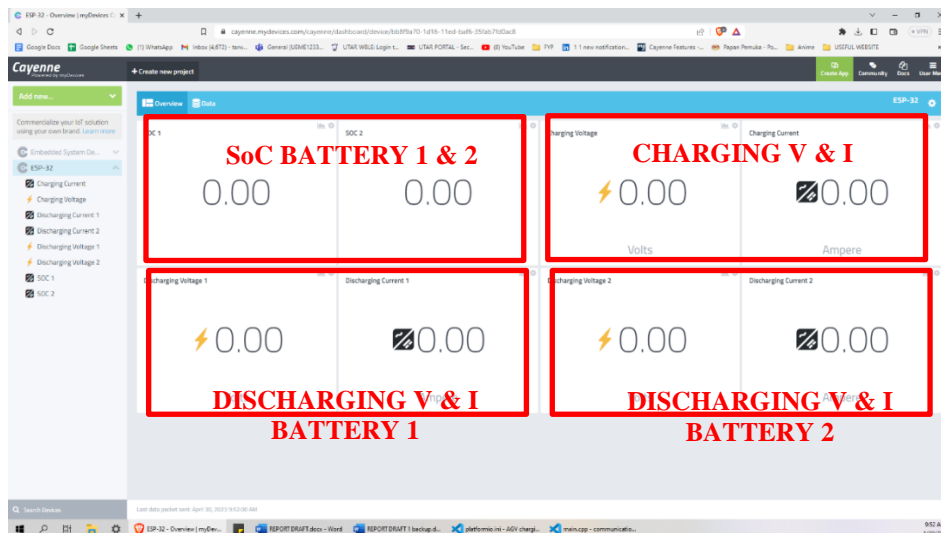


Figure 4.5: Cayenne data visualization

4.2.3 Autonomous charging parameter adjustment

Figure 4.6 shows the hardware for automating DPS5015, the jumper wire was connected to Arduino while one set of 8-pin wires was connected to DPS5015 and another 8-pin wire to the control panel.

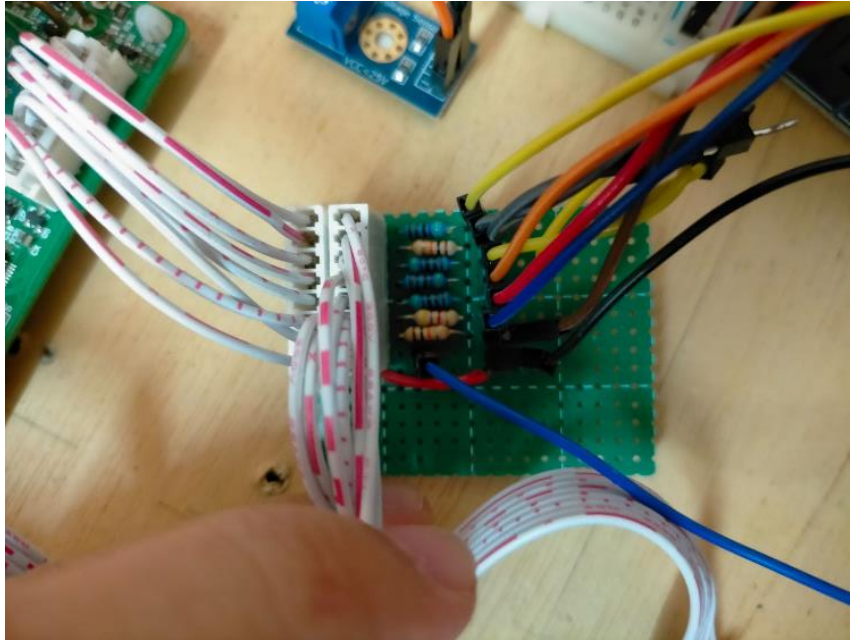


Figure 4.6: Wire extension from the control panel to Arduino

4.2.4 SoC estimator

Figure 4.7 shows the discharging circuit built for testing the SoC estimation, Figure 4.8 shows the SoC curve during the discharging and charging process while Figure 4.9 shows the voltage and current waveform against time during the entire discharging and charging process. Next, Table 4.1 summarizes Figure 4.8 and Figure 4.9 quantitatively.

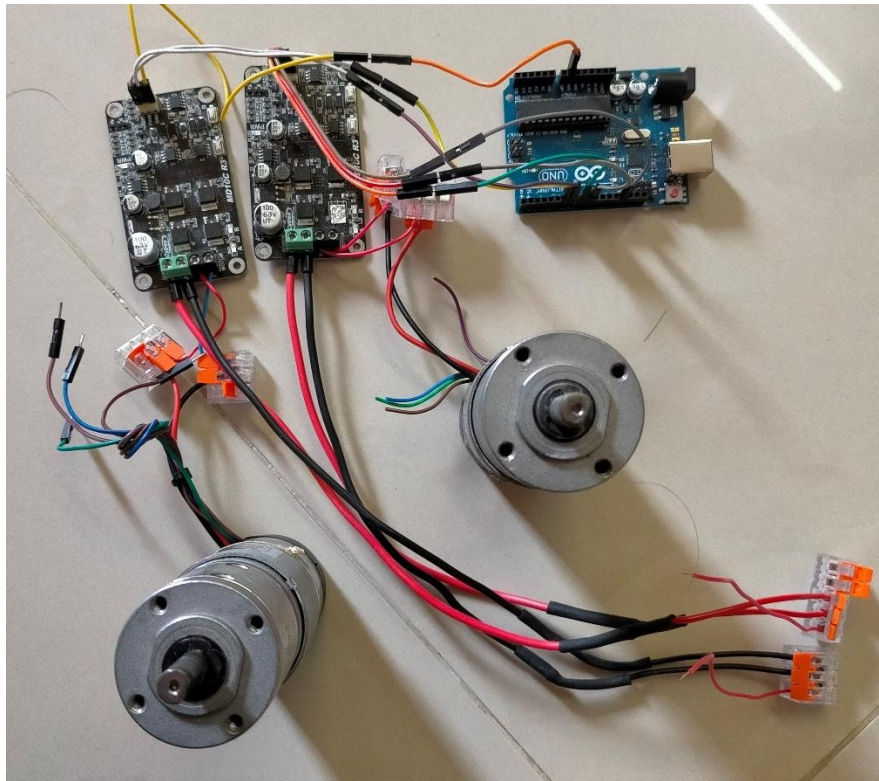


Figure 4.7: Discharging circuit

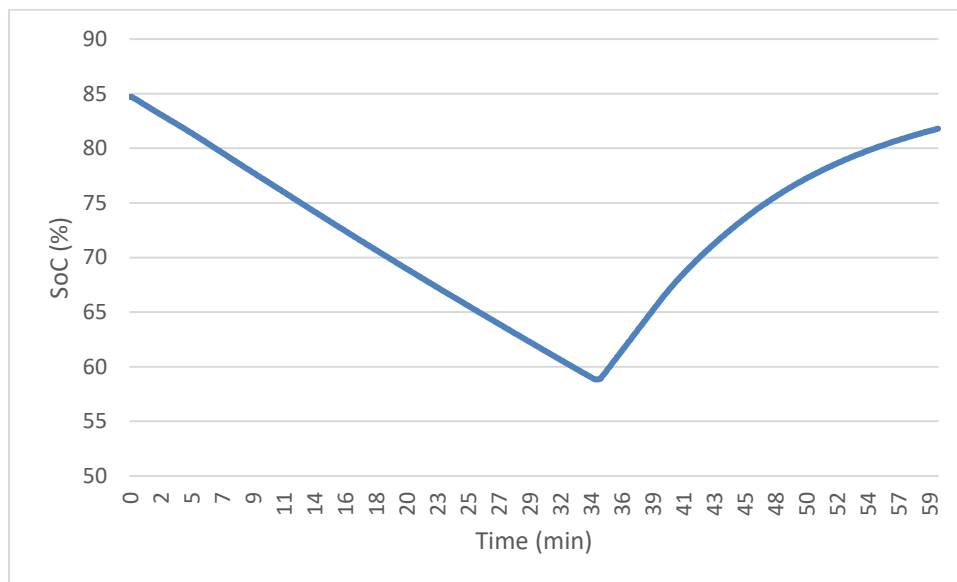


Figure 4.8: SoC curve for discharging and charging

Figure 4.9 shows the graph of voltage and current against time. The waveform from the beginning to 34 minutes shows the discharging waveform, while the waveform after 34 minutes shows the charging waveform done in CC-CV profiles.

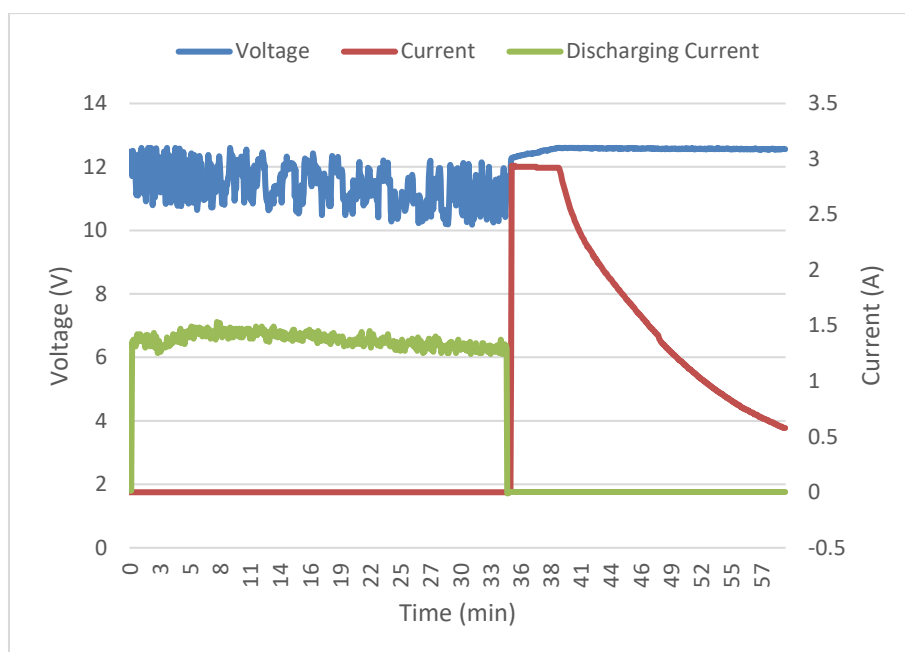


Figure 4.9: Voltage (V) and Current (A) vs Time (min) curve for Charging and Discharging process

Table 4.1: SoC for charging and discharging process

Initial SoC	84.7%
SoC after discharge	58.84%
Final SoC	81.79%
Discharge time (min)	34.27
Average discharge voltage (V)	11.15
Average discharge current (A)	1.31

4.3 Part 1 Discussion

4.3.1 Battery charging station's prototype

The current design of the charging station has been improved from the initial design proposed in FYP1. The initial design proposed in FYP1 involved using one BMS to charge two battery packs simultaneously, while the current design uses one BMS to charge one battery at a time. This change was made because it was found that BMS was designed to cater to one battery at a time. When multiple batteries are connected to the BMS, it can affect the BMS's performance in regulating the charges (DIY Solar Power, n.d.).

Additionally, the previous design used one set of current and voltage sensors for charging and discharging. However, the current design uses separate current and voltage sensors for charging and discharging. This is because it was found that during the charging process, current flows into the battery from both the main terminal (+ve and -ve) and the four BMS ports. Therefore, measuring the current from the main terminal alone would result in only a fraction of the actual current being sensed, as shown in Figure 4.10, where the current before BMS was 3.02A while the current after the BMS (measured from +ve and -ve terminals) was 0.44A. Besides that, measuring the charging voltage from the battery itself is inconsistent due to voltage fluctuations and zero drift caused by the BMS regulation function. For these reasons, the current design uses two sets of current and voltage sensors: one to sense the charging parameters before the BMS, and another to sense the discharging parameters after the BMS.

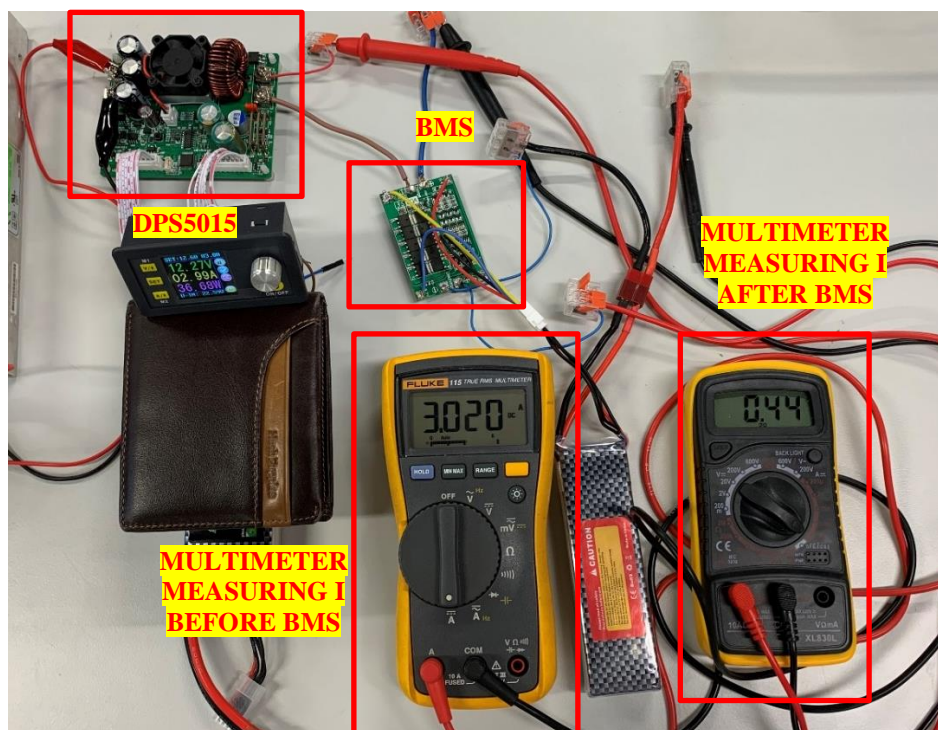


Figure 4.10: Differences between the current before and after BMS

As for IoT data management, ESP32 has successfully established connection and sends data to Cayenne website consistently without issue. The data storage function of Cayenne also works efficiently as shown in Figure 4.4.

and the user can export the data from Cayenne in an excel file with just a click of a button.

4.3.2 Autonomous charging parameter adjustment

Figure 4.6 shows the extension made to control the DPS5015 using Arduino. The jumper wires were connected to the digital pin of Arduino while one of the 8-pin wires was connected to the DPS5015 and the other 8-pin wire was connected to the control panel. With this extension, Arduino was able to control the DPS5015, however, it was found during testing that the increment and decrement function of the DPS5015 suffers random error. The increment and decrement functions were controlled by a mechanical rotary encoder in DPS5015, when the rotary encoder was rotated clockwise, it will perform increment while when it was rotated anticlockwise, it will perform decrement action. Similar to other buttons on the control panel, the rotary encoder was also low-triggered.

When programmed, sometimes Arduino was not able to control the rotary encoder. According to Professor Potter (2017), the rotary encoder has 30 detents per revolution but only 15 full quadrature pulses/rev, this causes the rotary encoder to be grounded once every two detents. Since Arduino controls the rotary encoder by grounding the wire, it can not control the rotary encoder if it was already grounded in the first place.

To overcome this issue, an additional wire was connected from the rotary encoder pin to Arduino. If the rotary encoder was in a grounded state, the LED on the Arduino will light up to inform the user to manually adjust the encoder to a “HIGH” state. When the encoder was in the “HIGH” state, it will remain in that state as long as the rotary encoder was not turned physically.

4.3.3 SoC estimation

In order to test the efficiency of the SoC estimator, an external discharging circuit consisting of a motor driver, DC motor, and Arduino Uno was built as shown in Figure 4.7. A charged battery with a known SoC was used to power the DC motor for a period of time, and then it was recharged using CC-CV with similar termination criteria. The accuracy of the SoC estimator was evaluated by how close the final SoC was to the initial SoC before discharging. According

to Figure 4.8 and Table 4.1, the discharge process stopped at 34.27 minutes while the charging process was from 34.27 to 58 minutes. The initial SoC was 84.7%, it discharged until the SoC was 58.84%, and then the battery was recharged using a similar charging profile and termination criteria: CC-CV-0.2c. After recharging, the SoC was 81.79%. The error for the SoC estimation was calculated using Equation (4.1).

$$Pt = V_s It(DOD)\eta \quad (4.1)$$

$$t = \frac{V_s It(DOD)\eta}{VI}$$

where

Steady state discharge voltage, $V_s = 11.1V$

Discharging voltage, $V = 11.15V$

Discharge current, $I = 1.31A$

Total ampere hour of battery, $It = 3Ah$

Depth of Discharge, $DOD = 84.7\% - 58.84\% = 25.86\%$

Efficiency, $\eta = 90\%$

Thus, the time needed for discharging the battery was:

$$t = \frac{(11.1V)(3Ah)(0.2586)(0.90)}{(11.15V)(1.31A)} = 0.533 \text{ hour} \approx 31.98 \text{ min}$$

Since the discharge time collected from the experiment was 34.27 min, the error for the SoC estimation was:

$$\text{Percentage Error (\%)} = \frac{34.27 \text{ min} - 31.98 \text{ min}}{31.98 \text{ min}} \times 100\% = 7.16\%$$

Thus, the SoC estimation error is 7.16%. A percentage error of 7.16% was acceptable as most industry SoC estimators only indicate the SoC of the battery every 20% or 25%. For example, the LiPo battery indicator from

TECHDIY indicates SoC every 20% interval (TECHDIY, n.d.), while the SoC estimator from China generally indicates SoC every 25% interval (meltsee, n.d.).

4.4 Part 2 Result: CC-CV and MSCC charging profile

In order to test the CC-CV and MSCC charging parameters, an IMAX B6 was used to discharge the battery. According to the specifications of the IMAX B6 charger, it fully discharged the LiPo battery to 0%. Before all the test charging was done, the LiPo battery was first discharged using the IMAX B6 charger to set a standard starting charge for all the batteries. Next, as stated in the methodology, CC-CV charged the battery at 1.0C (3A) and had a termination criterion of 0.2C (0.6A), while MSCC had current levels of 5.4A - 4.1A - 2.8A - 1.6A - 0.6A. The MSCC charging was considered completed when the final current level (0.6A) had been injected into the battery and the charging reached the CV phase with a drop in current of more than 0.03A. Figure 4.11, 4.12, 4.13, 4.14, 4.15, and 4.16 shows the SoC and graph of voltage and current against time for CC-CV charging for all three times charging while Table 4.2 summarizes all the result in quantitative value.

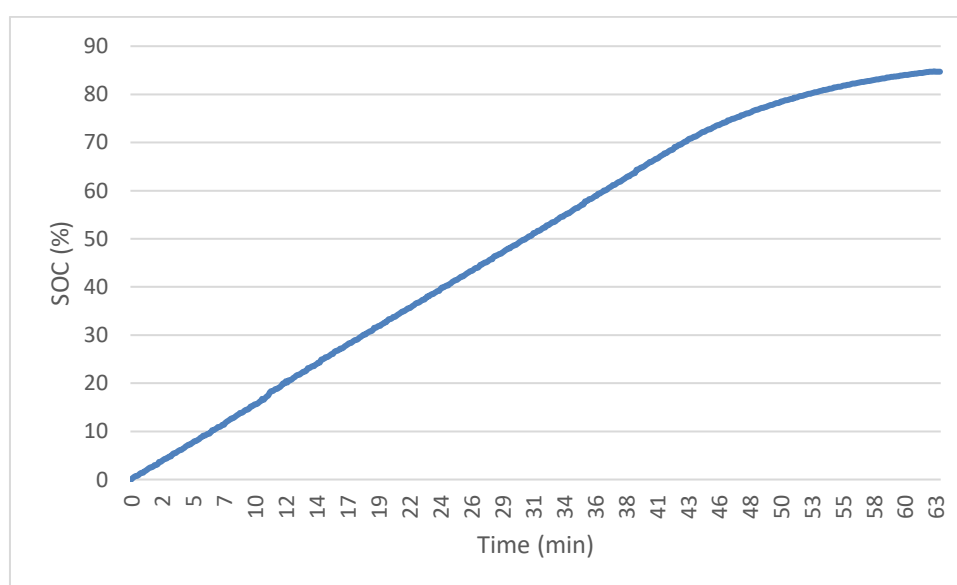


Figure 4.11: CC-CV CHARGE 1: SOC (%) vs Time (min)

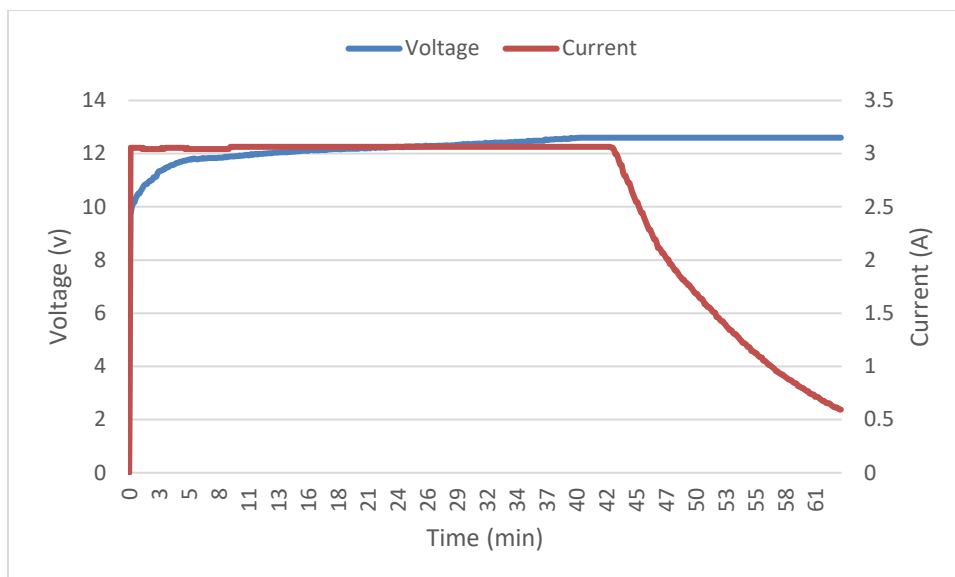


Figure 4.12: CC-CV CHARGE 1: Voltage (v) and Current (A) vs Time (min)

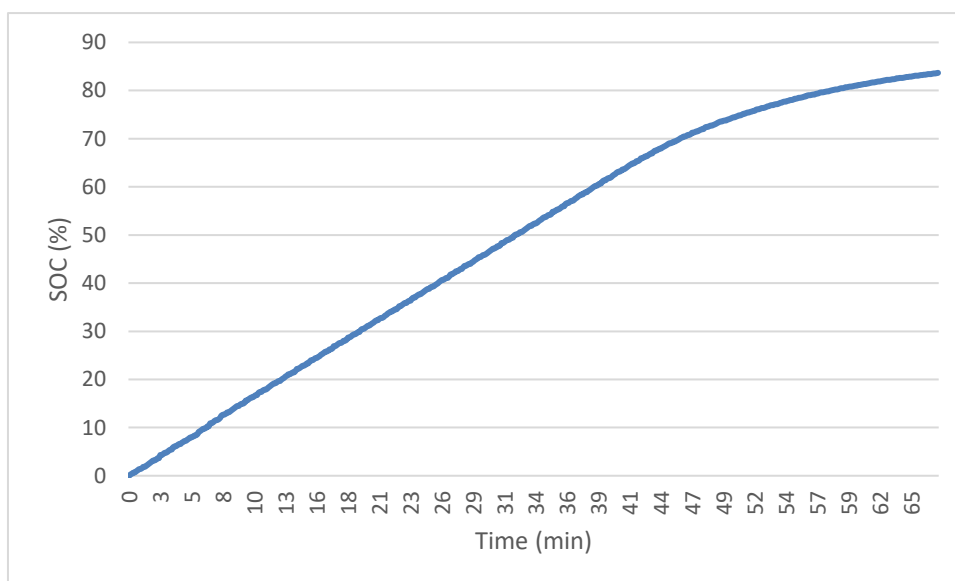


Figure 4.13: CC-CV CHARGE 2: SOC (%) vs Time (min)

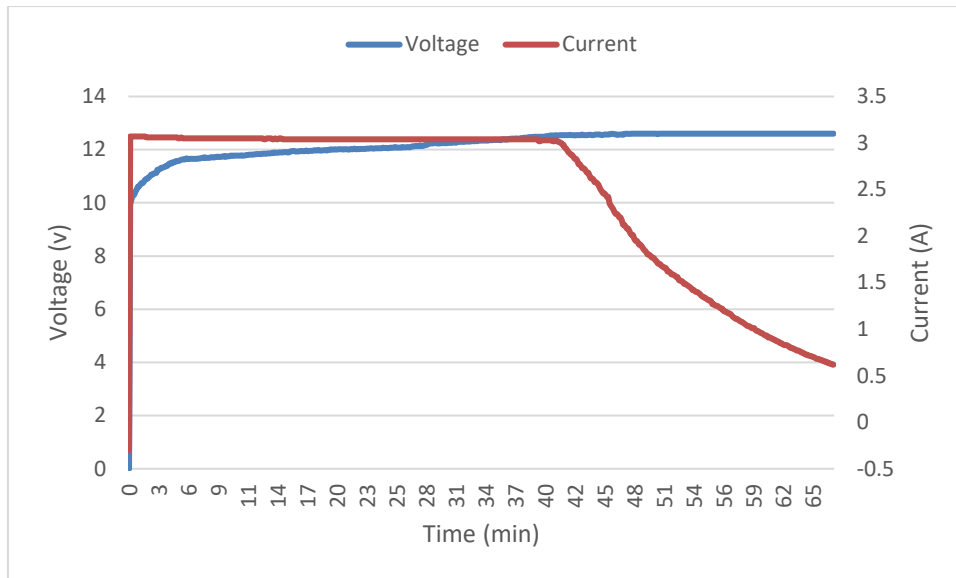


Figure 4.14: CC-CV CHARGE 2: Voltage (v) and Current (A) vs Time (min)

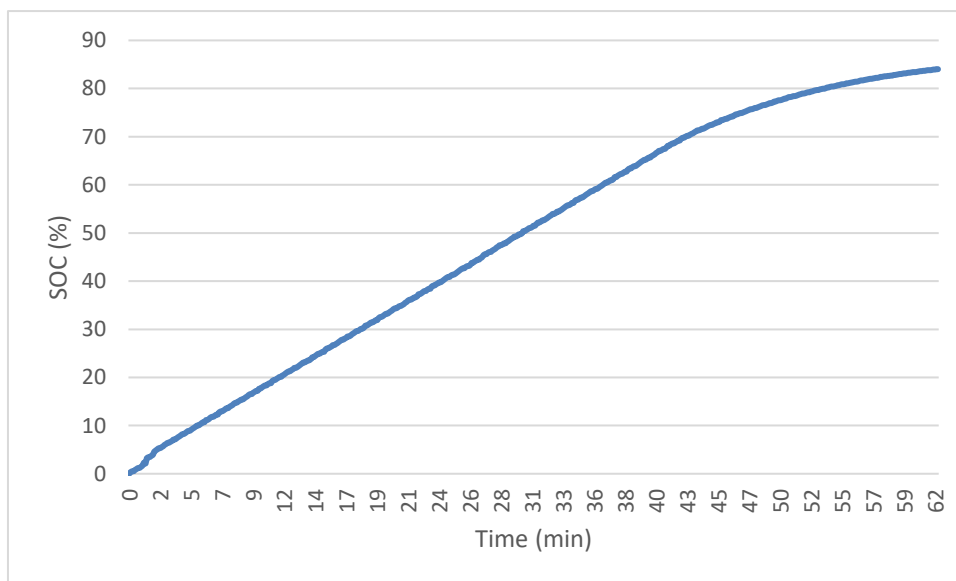


Figure 4.15: CC-CV CHARGE 3: SOC (%) vs Time (min)

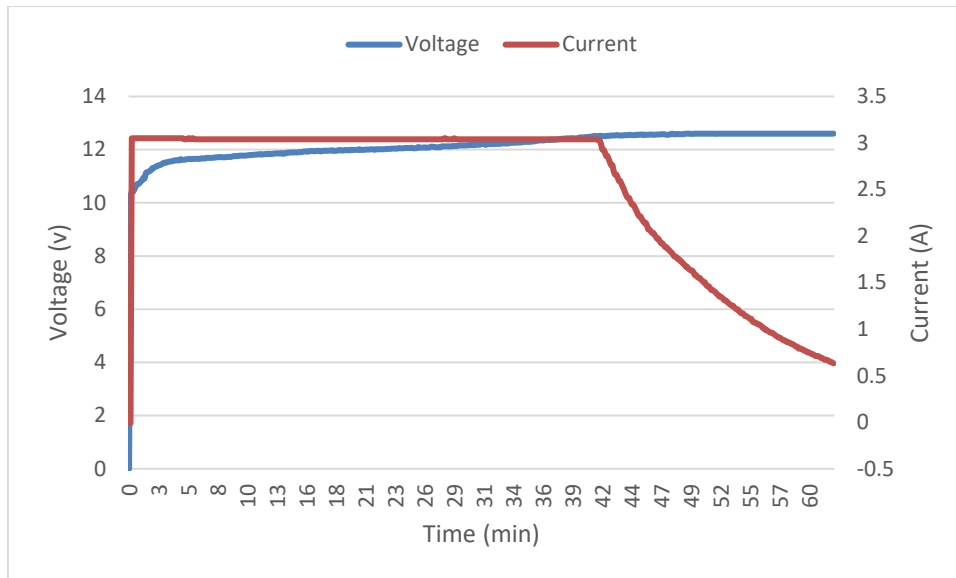


Figure 4.16: CC-CV CHARGE 3: Voltage (v) and Current (A) vs Time (min)

Table 4.2: CC-CV charging result

CC-CV	Charging time(min)	State of Charge (SOC)(%)	Time reaches CV phase (min)
Charge 1	62.86	84.70	42.82
Charge 2	65.76	83.67	41.07
Charge 3	61.92	84.02	41.36
Average	63.51	84.13	41.75

Figures 4.17, 4.18, 4.19, 4.20, 4.21, and 4.22 show the SoC and graph of voltage and current against time for MSCC charging for all the three times tested while Table 4.3 and Table 4.4 summarize all the results in quantitative value.

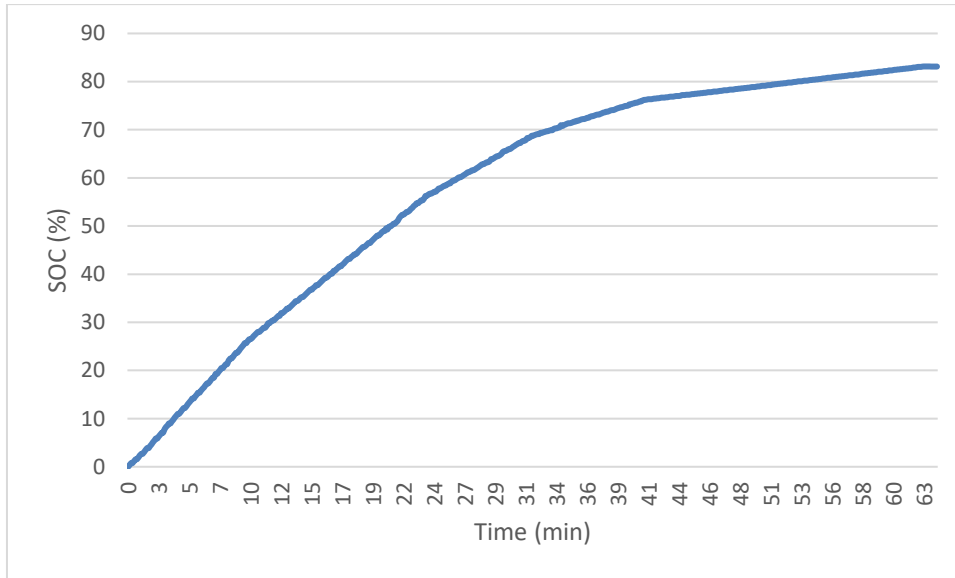


Figure 4.17: MSCC CHARGE 1: SOC (%) vs Time (min)

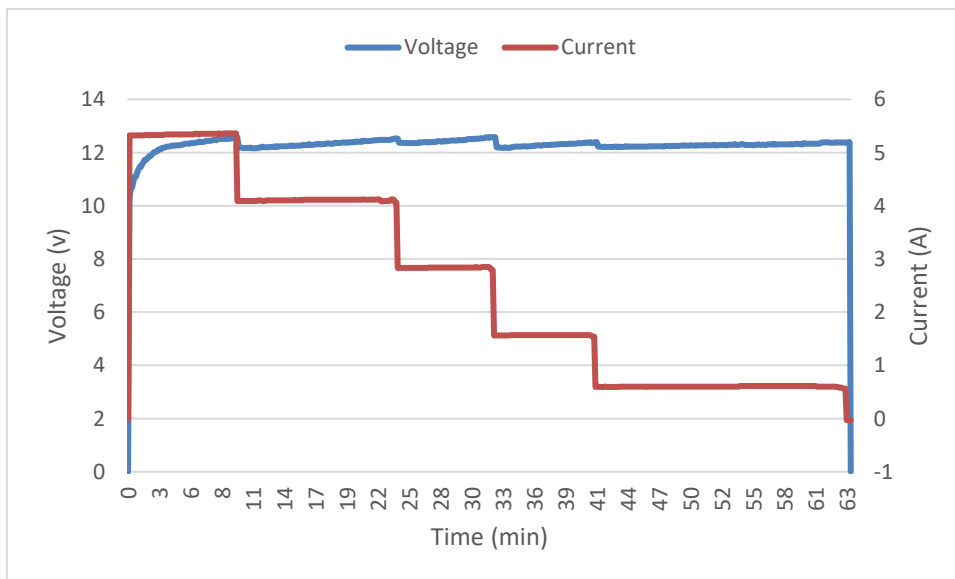


Figure 4.18: MSCC CHARGE 1: Voltage (v) and Current (A) vs Time (min)

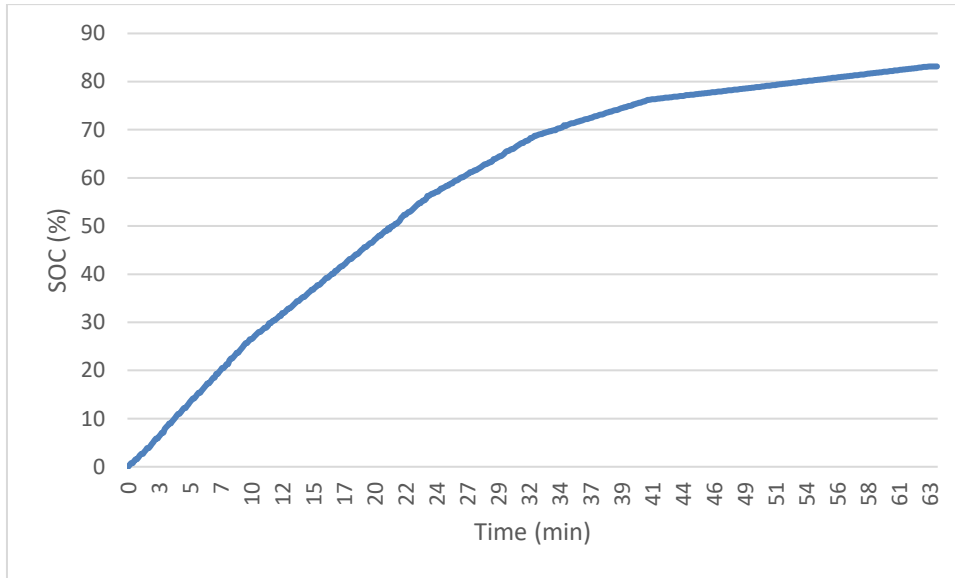


Figure 4.19: MSCC CHARGE 2: SOC (%) vs Time (min)

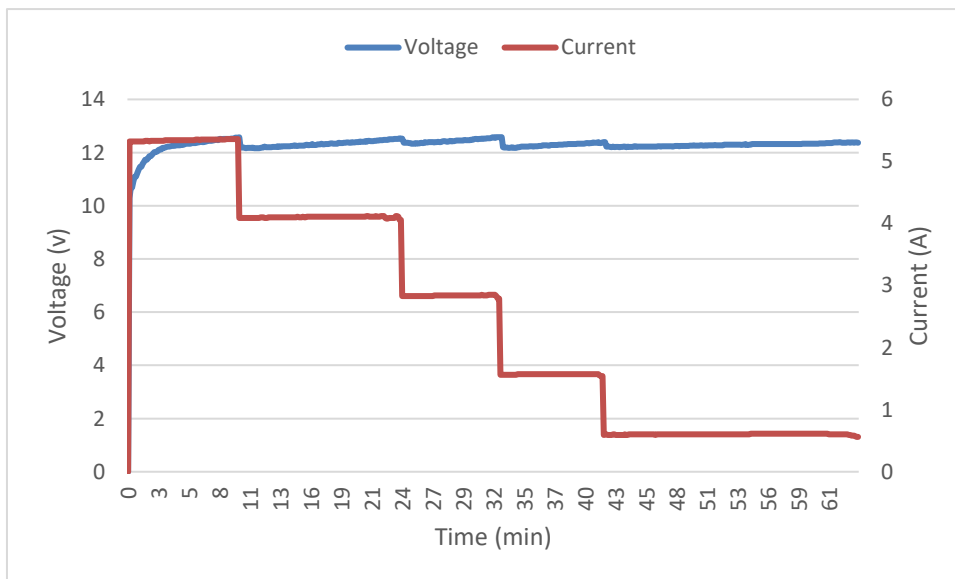


Figure 4.20: MSCC CHARGE 2: Voltage (v) and Current (A) vs Time (min)

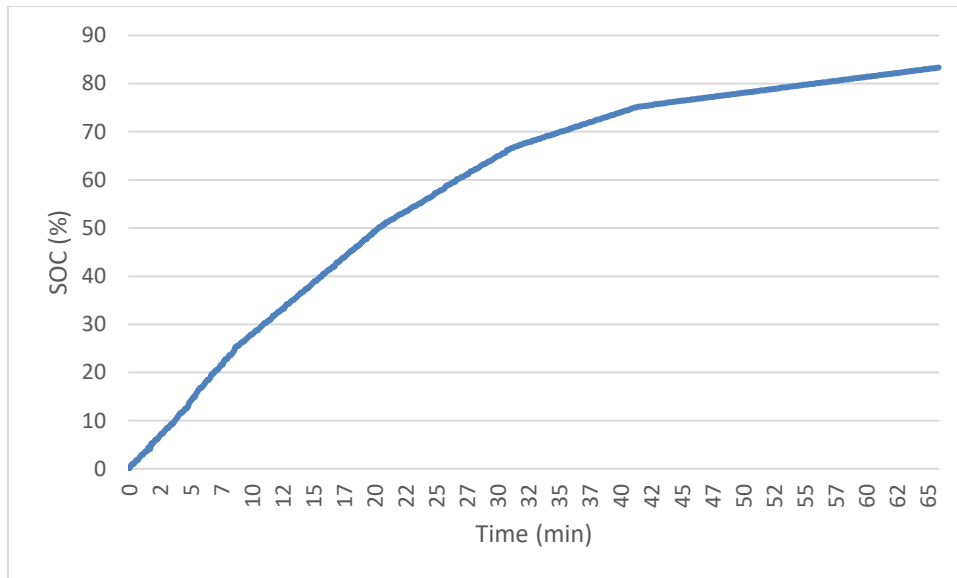


Figure 4.21: MSCC CHARGE 3: SOC (%) vs Time (min)

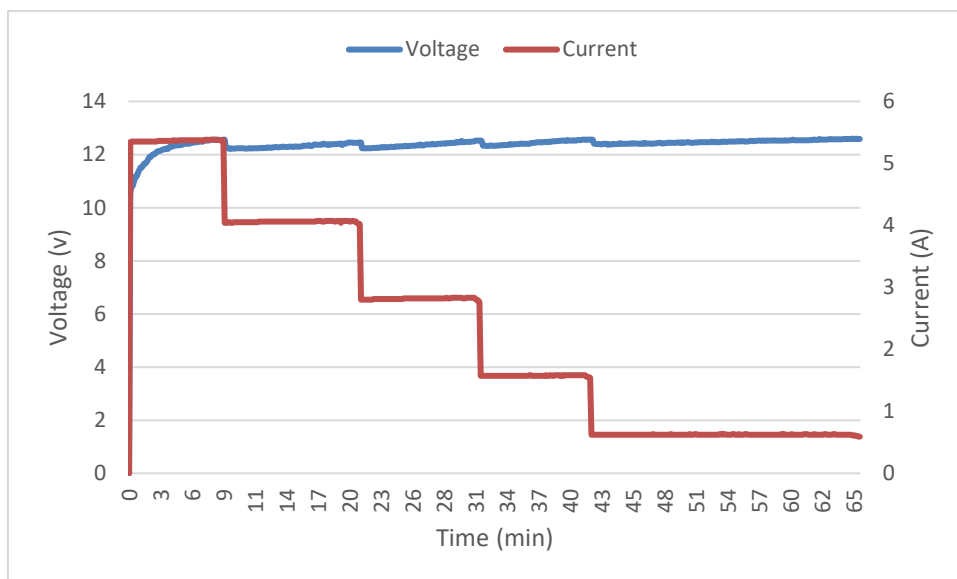


Figure 4.22: MSCC CHARGE 3: Voltage (v) and Current (A) vs Time (min)

Table 4.3: MSCC charging result

MSCC	Charging time(min)	State of Charge (SOC)(%)
Charge 1	63.83	83.13
Charge 2	63.71	83.14
Charge 3	65.87	83.33
Average	64.47	83.20

Table 4.4: MSCC charging interval

	Stage 1 (min)	Stage 2 (min)	Stage 3 (min)	Stage 4 (min)	Stage 5 (min)
Charge 1	9.64	14.12	8.50	8.95	22.62
Charge 2	9.60	13.99	8.79	9.02	22.31
Charge 3	8.52	12.26	10.67	9.88	24.54
Average	9.25	13.46	9.32	9.28	23.16

4.5 Part 2 Discussion

4.5.1 CC-CV charging

The CC-CV charging curve showed the correct waveform. During the constant current (CC) phase, the current was constant while the voltage slowly increased up until the cut-off voltage of 12.6V was reached. When the cut-off voltage was reached, the charging switched to the constant voltage (CV) phase, where the current slowly decreased until the termination current of 0.6A, while the voltage remained stable throughout the CV phase.

According to Table 4.2, the average charging time for the 3-test charge was 63.51 minutes, and it charged the battery from SoC 0% to 84.13. The charging process reached the CV phase at an average of 41.75 minutes, while the average charging time was 63.51 minutes. This meant that the CV phase only lasted for 21.76 minutes. The reason the CV phase was shorter than the CC phase was due to the high termination criteria of 0.2C. Compared to conventional CC-CV chargers which terminate at 0.1C, the CV phase would be much longer than the CC phase (Jha et al., 2022). Moreover, the same reason also applied to the lower SoC. The reason the SoC didn't go any higher was because of the high termination criteria, which was set at 0.2C (0.6A). If the termination criteria were lower, it would result in a higher SoC but a longer charging time (Jiang et al., 2020).

4.5.2 MSCC charging

On the other hand, the MSCC charging curve also showed the correct waveform where the charging started with CC while the voltage slowly increased up until the cut-off voltage, 12.60V. When the cut-off voltage was reached, the charger

changed the charging current to the next level. When the current had been adjusted, the charging voltage decreased to lower than the cut-off voltage automatically and the process was repeated.

Besides that, conventional MSCC uses the cut-off voltage to indicate when to change the current level during the charging process, however, the MSCC tested in this project changed the current level only after the charging had reached the CV phase of that level and had a current drop of more than 0.03A. This was because from the testing it was found that it was more reliable to wait until the charging reached the CV phase before changing the current level as compared to waiting until the cut-off voltage only.

According to Table 4.3, the average charging time was 64.47min while the SoC increment was from 0% to 83.20%. According to Table 4.4, the average charging time for each interval of MSCC (5.4A - 4.1A - 2.8A - 1.6A - 0.6A) was 9.25 min - 13.46 min – 9.32 min – 9.28 min – 23.16 min. The last current level consumed significantly more time as compared to all the other current levels. This was because the cut-off current of the last stage of MSCC had a significant effect on the charging time, the lower the cut-off charging current, the higher the charging time (Jiang et al., 2020).

4.5.3 Comparison between CC-CV and MSCC charging

According to Tables 4.2 and 4.3, the average charging time and average SoC are almost the same for both CC-CV and MSCC charging profiles, with CC-CV performing slightly better than MSCC profiles. The average charging time to reach the termination criteria for the CC-CV profile is 63.51 minutes with an SoC of 84.13%, while the MSCC profile is 64.47 minutes with an SoC of 83.20%. The reason the MSCC profile takes longer to charge and has a lesser SoC despite charging at multiple different current levels is because too much time was spent during the charging of the last current level. The MSCC profile spent 23.16 minutes charging at 0.6A, while CC-CV profiles already terminate the charging at 0.6A. This causes the difference in the performance of both charging profiles.

From the results shown, the OCP for the MSCC profile that was found by Jiang et al. (2020) did not result in a fast charging time since it has the same charging time as CC-CV charging profiles. This was because the charging

process was a trade-off between multiple indicators. Although the MSCC charging profile did not provide faster charging, it has high charging efficiency and significantly lower battery temperature rise during the charging process, which lessens the depletion of the health of the battery (Jiang et al., 2020).

4.6 Summary

In short, the battery charging station for AGV has been developed with all the functions tested and working well. Parts of the design for FYP1 have been improved and the latest charger design was able to perform better. The SoC estimator has an error of 7.16% which is within the acceptable range when compared with industrial SoC estimator.

Furthermore, the battery charging station was capable of performing CC-CV and MSCC charging profiles correctly. Comparisons between CC-CV and MSCC were made using real charging data instead of simulation and the result of comparison shows that CC-CV and MSCC at the reference OCP have almost similar charging performance while MSCC lessens the depletion of the health of the battery.

CHAPTER 5

CONCLUSIONS AND RECOMMENDATIONS

5.1 Conclusions

In short, the battery charging station for AGV has been successfully developed, consisting of important functions such as IoT data management, SoC estimator, and flexible charging adjustment. The design of the battery charging station was improved from the previous version proposed in FYP1. The current charging station is capable of performing more efficiently and reliably through the introduction of extra sets of current and voltage sensors before BMS and proper BMS usage. Moreover, the IoT data management, which comprises ESP32 transmitting data to Cayenne, proves its reliability by storing all the test data from CC-CV and MSCC charging, which were shown in Chapter 4. On the other hand, the SoC estimation was tested and showed a percentage error of 7.16%, which was acceptable when compared with other industrial SoC estimators.

Besides that, the study of CC-CV and MSCC charging conducted in Chapter 4: Part 2 Discussion was done using actual charging profiles. The results show that the charging station was able to perform CC-CV and MSCC charging profiles correctly. The OCP for the MSCC profiles that were chosen (5.4A - 4.1A - 2.8A - 1.6A - 0.6A) charges at an approximately similar speed to CC-CV-0.6A charging while lessening the depletion of the SoH of the battery. These comparison results were similar to the results obtained by Jiang et al. (2020) in their paper, thus proving the reliability of the battery charging station's prototype.

5.2 Recommendations for future work

Future work can involve adding the mechanical docking parts into the charging station and AGV itself. Firstly, the AC/DC converter will be separated and placed in the charging station while all the other components will be placed on the AGV. Next, connects the input power terminals of the DPS5015 to a suitable electrode. When the AGV docks with the charging station, the electrodes will be extended to establish a connection with the AC/DC power supply and thus start the charging process. This way the battery charging station for the AGV will be fully functional.

Next, the current battery charging station for AGV is very flexible as the charging adjustment can be done using Arduino and it also has a reliable data management system. With these functions, future work can involve exploring more alternative charging profiles such as pulse charging, multiple stage constant current-constant voltage (MSCCCV), and more.

REFERENCES

Analog, n.d. *Transform a DC/DC Converter into a High Performance, Full-Featured Battery Charger | Analog Devices*. [online] Available at: <<https://www.analog.com/en/education/education-library/videos/5579264755001.html>> [Accessed 3 August 2022].

Baccouche, I. *et al.* (2015) “Implementation of a Coulomb counting algorithm for SOC estimation of Li-ion battery for multimedia applications,” *2015 IEEE 12th International Multi-Conference on Systems, Signals & Devices (SSD15)* [Preprint]. Available at: <https://doi.org/10.1109/ssd.2015.7348255>.

Chen, M. and Rincon-Mora, G., 2006. Accurate, Compact, and Power-Efficient Li-Ion Battery Charger Circuit. *IEEE Transactions on Circuits and Systems II: Express Briefs*, 53(11), pp.1180-1184.

Cho, I.-H., Lee, P.-Y. and Kim, J.-H., 2019. Analysis of the Effect of the Variable Charging Current Control Method on Cycle Life of Li-ion Batteries. *Energies*, 12(15), 3023. Available at: <https://doi.org/10.3390/en12153023>

Digikey, 2022. *AP4305KTR-G1 Diodes Incorporated | Integrated Circuits (ICs) | DigiKey*. [online] Available at: <https://www.digikey.com/en/products/detail/AP4305KTR-G1/AP4305KTR-G1DICT-ND/8545801?WT.z_cid=ref_netcomponents_dkc_buynow&utm_source=netcomponents&utm_medium=aggregator&utm_campaign=buynow> [Accessed 10 August 2022].

Digikey, 2022. *MP26085DJ-LF-Z Monolithic Power Systems Inc. | Integrated Circuits (ICs) | DigiKey*. [online] Available at: <<https://www.digikey.com/en/products/detail/monolithic-power-systems-inc/MP26085DJ-LF-Z/9555324>> [Accessed 10 August 2022].

docooler.os (no date) *{doc} Waterproof Battery SOC Power Meter Capacity Indicator 8-100V Direct Current Voltmeter 12.0V 24V 36V 48V 60V 72V Lithium Iron, Shopee.com.my*. Available at: https://shopee.com.my/-doc-Waterproof-Battery-SOC-Power-Meter-Capacity-Indicator-8-100V-Direct-Current-Voltmeter-12.0V-24V-36V-48V-60V-72V-Lithium-Iron-Phosphate-Battery-Ternary-Lithium-Polymer-Battery-i.283370085.20376231609?sp_atk=cdf23cfc-1b90-47ec-9b3d-c4ded7ec7451&xptdk=cdf23cfc-1b90-47ec-9b3d-c4ded7ec7451 (Accessed: April 30, 2023).

ElectronicsTutorials, n.d. *Switch Mode Power Supply*. [online] Available at: <<https://www.electronics-tutorials.ws/power/switch-mode-power-supply.html>> [Accessed 12 July 2022].

Fuqiang, A. *et al.* (2019) “Multi-stage constant-current charging protocol for a high-energy-density pouch cell based on a 622ncm/graphite system,” *RSC Advances*, 9(37), pp. 21498–21506. Available at: <https://doi.org/10.1039/c9ra03629f>.

Ghaeminezhad, N. and Monfared, M., 2021. Charging control strategies for lithium-ion battery packs: Review and recent developments. *IET Power Electronics*, 15(5), pp.349-367.

Hareendran, T.K., n.d. *3.7V Li-Ion Battery Charger Circuit*. [online] ELECTRO SCHEMATICS. Available at: <https://www.electroschematics.com/3-7v-li-ion-battery-charger-circuit/> [Accessed 26 July 2022].

Jha, B., Mallik, B., Basnet, S., Yadav, A. and Prasad Pandey, R., 2022. Design and Simulation of Different Variants of Charging Lithium-Ion Batteries in Search for Optimum Charging Algorithm. In: *2022 4th International Conference on Smart Systems and Inventive Technology (ICSSIT)*. [online] Available at: <https://ieeexplore-ieee-org.libezp2.utar.edu.my/document/9716535/references> [Accessed 12 June 2022].

Jiang, L. *et al.* (2020) “Optimization of multi-stage constant current charging pattern based on Taguchi method for Li-Ion Battery,” *ScienceDirect*, 259, p. 114148. Available at: <https://doi.org/10.1016/j.apenergy.2019.114148>.

Life Hacker (no date) *How to exchange data between Arduino and ESP32 using serial communication?*, *Programming Boss: Programming for Beginners*. Blogger. Available at: <https://www.programmingboss.com/2021/04/esp32-arduino-serial-communication-with-code.html#gsc.tab=0> (Accessed: April 30, 2023).

Lim, C., Mandal, D., Bakkaloglu, B. and Kiaei, S., 2021. Switching Battery Charger with Cascaded Two Loop Control Using Time-Based Techniques. In: *2021 IEEE Applied Power Electronics Conference and Exposition (APEC)*. [online] IEEE. Available at: <https://ieeexplore-ieee-org.libezp2.utar.edu.my/document/9487236> [Accessed 13 July 2022].

meltsee (no date) *1/2/3/4/5/6/7/8S Lithium Battery Capacity Indicator Module Blue Green Display Electric Vehicle Battery Power Tester 3.7V Li-ion*, *Shopee.com.my*. Available at: https://shopee.com.my/1-2-3-4-5-6-7-8S-Lithium-Battery-Capacity-Indicator-Module-Blue-Green-Display-Electric-Vehicle-Battery-Power-Tester-3.7V-Li-ion-i.110910897.4231678241?sp_atk=76ca8ddf-9f60-4446-a1c1-400a128f07ac&xptdk=76ca8ddf-9f60-4446-a1c1-400a128f07ac (Accessed: April 30, 2023).

Potter, S. and Instructables (2017) *Power Supply Automation: DPS5015, DP50V5A controlled by Arduino -- professor potter*, *Instructables*.

Instructables. Available at: <https://www.instructables.com/Power-Supply-Automation-DPS5015-DP50V5A-Controlled/> (Accessed: April 30, 2023).

Powerint, 2012. *RDR-313 - 30 W Single Output Flyback Converter | Power Integrations, Inc.* [online] Available at: <https://www.powerint.cn/design-support/design-examples/rdr-313-30-w-single-output-flyback-converter> [Accessed 18 August 2022].

Powerint, 2016. *DER-453 - 45 W Single Output Secondary Side Regulated Converter | Power Integrations, Inc.* [online] Available at: <https://www.powerint.cn/design-support/design-examples/der-453-45-w-single-output-secondary-side-regulated-converter> [Accessed 25 August 2022].

Powerint, 2021. *DER-915 - 84 W High-Line Input Charger with 93% Efficiency using InnoSwitch3-CP with PowiGaN Technology | Power Integrations, Inc.* [online] Available at: <https://www.powerint.cn/design-support/design-examples/der-915-84watt-charger-93pct-efficiency-using-innoswitch3-cp-powigan> [Accessed 18 August 2022].

PowerTech (no date) *Lithium-ion state of charge (SOC) measurement - coulomb counter method - OCV, PowerTech Systems - PowerTech Systems.* Available at: <https://www.powertechsystems.eu/home/tech-corner/lithium-ion-state-of-charge-soc-measurement/> (Accessed: April 30, 2023).

Renhotec Technology (2022) *Ev charging: Slow vs fast charging, LinkedIn.* Available at: <https://www.linkedin.com/pulse/ev-charging-slow-vs-fast-shenzhen-renhotec-technology-elect/> (Accessed: April 30, 2023).

Shen, W., Tu Vo, T. and Kapoor, A., 2012. Charging algorithms of lithium-ion batteries: An overview. In: *2012 7th IEEE Conference on Industrial Electronics and Applications (ICIEA)*. [online] Available at: <https://ieeexplore-ieee-org.libezp2.utar.edu.my/document/6360973/citations?tabFilter=papers#cite> [Accessed 12 June 2022].

Spiazzi, G. and Buso, S., 2002. Comparison between two single-switch isolated flyback and forward high-quality rectifiers for low power applications. In: *APEC. Seventeenth Annual IEEE Applied Power Electronics Conference and Exposition (Cat. No.02CH37335)*. [online] Available at: <https://ieeexplore-ieee-org.libezp2.utar.edu.my/document/989255> [Accessed 14 July 2022].

Super User, n.d. *AGV Wireless Charging? Manufacturers? Cost? Advantages?*. [online] Agvnetwork.com. Available at: <https://www.agvnetwork.com/wireless-charging-for-agv-and-autonomous-mobile-robots> [Accessed 18 August 2022].

TECHDIY (no date) *2S-8S 18650 Li-ion Lipo Lithium 5-30V Lead Acid Battery Level Indicator Tester LCD Display Meter Module Capacity Voltage Meter, Shopee.com.my.* Available at: <https://shopee.com.my/2S-8S-18650-Li-ion-Lipo-Lithium-5-30V-Lead-Acid-Battery-Level-Indicator-Tester-LCD-Display-Meter-Module-Capacity-Voltage-Meter->

[i.602915340.23922704824?sp_atk=9c37960c-4943-4d69-8e54-6aacbf430178&xptdk=9c37960c-4943-4d69-8e54-6aacbf430178](https://ieeexplore-ieee-org.libezp2.utar.edu.my/document/9338942?sp_atk=9c37960c-4943-4d69-8e54-6aacbf430178&xptdk=9c37960c-4943-4d69-8e54-6aacbf430178) (Accessed: April 30, 2023).

Yin, Q., Gan, J., Chen, T., Shi, W., Liu, X. and Chang, Z., 2020. Research on the flyback switch power supply based on the primary feedback and the valley control. In: *2020 IEEE 9th Joint International Information Technology and Artificial Intelligence Conference (ITAIC)*. [online] Available at: <<https://ieeexplore-ieee-org.libezp2.utar.edu.my/document/9338942>> [Accessed 12 June 2022].

APPENDICES

Appendix A: Code and sample excel file from Cayenne

Due to lengthy result, refer to the google drive link to access coding for Arduino and ESP32 microcontroller, and sample data downloaded from Cayenne.

<https://drive.google.com/drive/folders/1SUZPRVeUwWIZEUnDe7X5Czkxlgrix9nc?usp=sharing>